ECCOMAS Congress 2016
VII European Congress on Computational Methods in Applied Sciences and Engineering
M. Papadrakakis, V. Papadopoulos, G. Stefanou, V. Plevris (eds.)
Crete Island, Greece, 5–10 June 2016

MIXED INTEGRATORS FOR STRUCTURE-PRESERVING SIMULATIONS IN NONLINEAR STRUCTURAL DYNAMICS

Alexander Janz[1], **Peter Betsch**[1] **and Christian Hesch**[1]

[1]Institute of Mechanics
Karlsruhe Institute of Technology (KIT)
Otto-Ammann-Platz 9
76131 Karlsruhe, Germany
{alexander.janz, peter.betsch, christian.hesch}@kit.edu

Keywords: finite element methods; nonlinear elastodynamics; implicit; structure preserving

Abstract. *The present work deals with the design of structure-preserving numerical methods in the field of nonlinear elastodynamics and structural dynamics. Structure-preserving schemes such as energy-momentum consistent (EMC) methods are known to exhibit superior numerical stability and robustness. Most of the previously developed schemes are relying on a displacement-based variational formulation of the underlying mechanical model. In contrast to that we present a mixed variational framework for the systematic design of EMC schemes. The newly proposed mixed approach accomodates high-performance mixed finite elements such as the brick element due to Kasper & Taylor [15]. Accordingly, the proposed approach makes possible the structure-preserving extension to the dynamic regime of mixed high-performance elements. Numerical examples demonstrate the advantageous properties of the newly developed numerical methods resulting from the structure-preserving discretization in space and time.*

1 Introduction

Energy-momentum consistent (EMC) time-stepping schemes and their energy-decaying variants have been primarily developed in the framework of nonlinear structural dynamics. This type of structure-preserving integrators is known to exhibit superior numerical stability and robustness [12]. Previous developments of EMC schemes have been essentially confined to displacement-based finite elements. We refer to [30, 9, 24, 6, 2, 19, 18, 25],[29, 32, 16, 20, 7, 23, 8, 4] and [28, 11, 17, 5, 1, 13] for representative developments in the framework of nonlinear beams, shells and continua, respectively.

In this connection we remark that often applied finite element techniques such as selectively reduced integration, assumed natural strain interpolations and enhanced assumed strain approximations based on incompatible displacement modes essentially do not affect the design of EMC schemes[1]. In fact, second-order accurate EMC integrators typically rely on a mid-point type discretization of the weak form of the balance of linear momentum in conjunction with the introduction of an algorithmic stress formula [22].

To the best of our knowledge, a general framework for the design of EMC schemes for truly mixed nonlinear finite elements has not been accomplished so far. We refer to [3] for a mixed variational formulation for nonlinear structural dynamics which provides a natural framework for the EMC discretization in time. The EMC scheme in [3] is restricted to mixed finite elements, based on a Hu-Washizu type variational formulation in terms of displacements, Green-Lagrangian strains and conjugated stresses.

In the present work we newly present a Hu-Washizu type mixed variational formulation along with its EMC temporal discretization. Our developments start from a 6-field extension of Hamilton's principle that relies on the displacements, velocities, deformation gradient, right Cauchy-Green deformation tensor and the components of both the 1st and 2nd Piola-Kirchhoff stress tensor. The proposed 6-field variational principle can be linked to Liven's theorem [21, Sec. 26.2] and the Hu-Washizu principle [31]. The corresponding Euler-Lagrange equations provide the mixed variational formulation for the EMC discretization in time. The resulting mixed semi-discrete formulation can be used to develop EMC schemes for mixed finite elements relying on independent interpolations as named above.

We apply the newly developed mixed framework for the design of EMC integrators to the high-performance mixed-enhanced element developed by Kasper & Taylor [15]. This element exhibits superior coarse mesh accuracy along with a locking-free response in the incompressible limit. We refer to [14, 15] for further investigations in this direction. Given the commonly observed numerical stability and robustness of EMC

[1] This remark excludes the broader class of assumed strain methods for nearly incompressible problems in nonlinear elastodynamics investigated in [1], see also [11]

integrators, the mixed-enhanced element [15] can be regarded as ideal candidate for the EMC extension to the transient regime. The resulting structure-preserving numerical method can be expected to allow stable simulations on coarser space-time grids compared to standard methods. Furthermore we even obtain physically meaningful results for quasi incompressible material.

An outline of the rest of the paper is as follows. In Section 2 we present the basic notation and introduce our six-field formulation which provides the Euler-Lagrange equations needed for the subsequent discretization process. The design of a structure-preserving time-stepping scheme is treated in Section 3. The present approach to the design of EMC integrators is then further developed in the framework of the mixed-enhanced formulation in Section 4. After the presentation of numerical examples in Section 5, conclusions are drawn in Section 6.

2 Continuum Mechanics

We start our developments by an introduction of the notation of the applied continuum approach. After that, we introduce our mixed framework for the design of EMC integrators. At the end of this section, the conservation properties will be shown.

2.1 Notation

We consider a motion of a continuum body from the reference configuration $\mathcal{B} \in \mathbb{R}^3$ to the current configuration $\boldsymbol{\varphi}(\mathcal{B})$. This motion can be identified as a time-dependent continuous differentiable function $\boldsymbol{\varphi} \in \mathcal{U}$, where

$$\mathcal{U} := \{\boldsymbol{\varphi} : \mathcal{B} \times [t_0, t_e] \to \mathbb{R}^3 : \boldsymbol{\varphi} \in H^1(\mathcal{B}) \text{ and } \boldsymbol{\varphi}\big|_{\partial\mathcal{B}_\varphi} = \bar{\boldsymbol{\varphi}}\} \tag{1}$$

with the time-interval $[t_0, t_e]$ during the motion. We label material points by $\mathbf{X} \in \mathcal{B}$ and the material velocity is labeled by $\mathbf{V} \in \mathcal{V}$, with

$$\mathcal{V} := \{\delta\boldsymbol{\varphi} : \mathcal{B} \times [t_0, t_e] \to \mathbb{R}^3 : \delta\boldsymbol{\varphi} \in H^1(\mathcal{B}) \text{ and } \delta\boldsymbol{\varphi}\big|_{\partial\mathcal{B}_\varphi} = 0\} \tag{2}$$

Furthermore, the smooth boundary of the body can be partitioned into two parts, where

$$\boldsymbol{\varphi} = \bar{\boldsymbol{\varphi}} \quad \text{on} \quad \partial\mathcal{B}_\varphi \qquad \text{and} \qquad \widetilde{\mathbf{P}}\,\mathbf{N} = \bar{\mathbf{t}} \quad \text{on} \quad \partial\mathcal{B}_\sigma \tag{3}$$

with the prescribed motion of the body $\bar{\boldsymbol{\varphi}}$, the first non-symmetric Piola-Kirchhoff stress tensor $\widetilde{\mathbf{P}} \in \mathcal{M}$, the unit outward normal field $\mathbf{N}$ and the traction vector $\bar{\mathbf{t}}$. The space of $\widetilde{\mathbf{P}}$ is defined as

$$\mathcal{M} = \{\widetilde{\mathbf{P}} : \mathcal{B} \times [t_0, t_e] \to \mathbb{R}^{3\times 3} : \widetilde{P}_{iI} \in L^2(\mathcal{B})\} \tag{4}$$

We assume, that

$$\partial\mathcal{B} = \overline{\partial\mathcal{B}_\varphi \cup \partial\mathcal{B}_\sigma} \quad \text{and} \quad \partial\mathcal{B}_\varphi \cap \partial\mathcal{B}_\sigma = \emptyset \tag{5}$$

To describe the deformation of the body, we introduce the deformation gradient

$$\widetilde{\mathbf{F}} = \mathrm{Grad}\,\boldsymbol{\varphi}(\mathbf{X},t) = \frac{\partial \boldsymbol{\varphi}(\mathbf{X},t)}{\mathbf{X}} = D\boldsymbol{\varphi} \tag{6}$$

and its determinant as $j = \det\widetilde{\mathbf{F}} > 0$, where $\widetilde{\mathbf{F}} \in \mathcal{M}$. The right Cauchy-Green deformation tensor defines a measure of strain and can be written as

$$\widetilde{\mathbf{C}} = \widetilde{\mathbf{F}}^{\mathrm{T}}\,\widetilde{\mathbf{F}} \tag{7}$$

where $\widetilde{\mathbf{C}} \in \mathcal{M}$. Next we introduce the stress tensors that are work conjugate to the deformation gradient $\widetilde{\mathbf{F}}$ and the right Cauchy-Green deformation tensor $\widetilde{\mathbf{C}}$. We use the stored energy function $\hat{W}(\widetilde{\mathbf{F}})$ or $\bar{W}(\widetilde{\mathbf{C}})$ to define the stress and strain relations by

$$\widetilde{\mathbf{P}} = \frac{\partial \hat{W}(\widetilde{\mathbf{F}})}{\partial \widetilde{\mathbf{F}}} \quad \text{and} \quad \widetilde{\mathbf{S}} = 2\,\frac{\partial \bar{W}(\widetilde{\mathbf{C}})}{\partial \widetilde{\mathbf{C}}} \tag{8}$$

with the first Piola-Kirchhoff stress tensor $\widetilde{\mathbf{P}}$ as introduced above and the symmetric second Piola-Kirchhoff stress tensor $\widetilde{\mathbf{S}} \in \mathcal{M}$.

The equations of motion can be derived by imposing the condition of stationarity to

$$S(\boldsymbol{\varphi},\mathbf{V}) = \int_{t_0}^{t_e} \left(L(\boldsymbol{\varphi},\mathbf{V}) + (\dot{\boldsymbol{\varphi}} - \mathbf{V}) \cdot \partial_V L(\boldsymbol{\varphi},\mathbf{V})\right)\,\mathrm{d}t \tag{9}$$

for arbitrary variations of the state-space coordinates $(\boldsymbol{\varphi},\mathbf{V}) \in \mathbb{R}^3 \times \mathbb{R}^3$ in the time interval $[t_0,t_e]$. Note that in (9), Hamiltons principle is linked to Livens theorem (see, for example, Pars [21, Sec. **26.2 Liven's theorem**]). The aforementioned Lagrangian is defined as the difference between the kinetic and potential energy as $L(\boldsymbol{\varphi},\mathbf{V}) = T(\mathbf{V}) - V(\boldsymbol{\varphi})$. The kinetic energy of the body is given by

$$T(\mathbf{V}) = \int_{\mathcal{B}} \frac{1}{2}\mathbf{V} \cdot \rho_0 \mathbf{V}\mathrm{d}V \tag{10}$$

where $\rho_0 : \mathcal{B} \to \mathbb{R}$ is the reference density. We admit the decomposition of the potential energies in an internal and external part as

$$V(\boldsymbol{\varphi}) = V_{\mathrm{int}}(\widetilde{\mathbf{C}}(\boldsymbol{\varphi})) + V_{\mathrm{ext}}(\boldsymbol{\varphi}) \tag{11}$$

The external potential energy can be written as

$$V_{\mathrm{ext}} = -\int_{\mathcal{B}} \bar{\mathbf{b}} \cdot \boldsymbol{\varphi}\,\mathrm{d}V - \int_{\partial\mathcal{B}_\sigma} \bar{\mathbf{t}} \cdot \boldsymbol{\varphi}\,\mathrm{d}A \tag{12}$$

where $\bar{\mathbf{b}} : \mathcal{B} \to \mathbb{R}^3$ is the reference body force. In the following we focus on body forces only, so that the second term in (12) will not be considered in the sequel. For a stored energy function $\bar{W}(\widetilde{\mathbf{C}})$, the potential of the internal energy is assumed to be given by

$$V_{\mathrm{int}} = \int_{\mathcal{B}} \bar{W}(\widetilde{\mathbf{C}}(\boldsymbol{\varphi}))\,\mathrm{d}V \tag{13}$$

2.2 Hu-Wahizu type formulation

Instead of a two-field functional (9), we now consider an extension of the original Hu-Washizu variational [31] to a six-field formulation given by

$$\begin{aligned} S_{\mathrm{HW}}(\boldsymbol{\varphi},\mathbf{V},\mathbf{F},\mathbf{P},\mathbf{C},\mathbf{S}) = \int_{t_0}^{t_e} \Big[T(\mathbf{V}) - \big(V_{\mathrm{int}}(\mathbf{C}) + V_{\mathrm{ext}}(\boldsymbol{\varphi})\big) + (\dot{\boldsymbol{\varphi}} - \mathbf{V}) \cdot DT(\mathbf{V}) \\ - \int_{\mathcal{B}} \big(\mathbf{P} : \mathbf{g}^P(\boldsymbol{\varphi},\mathbf{F}) + \mathbf{S} : \mathbf{g}^S(\mathbf{F},\mathbf{C})\big)\,\mathrm{d}V \Big]\,\mathrm{d}t \\ = \int_{t_0}^{t_e} \int_{\mathcal{B}} \Big((\dot{\boldsymbol{\varphi}} - \frac{1}{2}\mathbf{V})\,\rho_0\,\mathbf{V} \Big)\,\mathrm{d}V\,\mathrm{d}t - \int_{t_0}^{t_e} V_{\mathrm{ext}}(\boldsymbol{\varphi})\,\mathrm{d}t \\ - \int_{t_0}^{t_e} \int_{\mathcal{B}} \big(W(\mathbf{C}) + \mathbf{P} : \mathbf{g}^P(\boldsymbol{\varphi},\mathbf{F}) + \mathbf{S} : \mathbf{g}^S(\mathbf{F},\mathbf{C})\big)\,\mathrm{d}V\,\mathrm{d}t \end{aligned} \tag{14}$$

where the energies are defined by (10), (12) and (13), respectively. The algebraic constraints in (14) can be written as

$$\begin{aligned} \mathbf{g}^P(\boldsymbol{\varphi},\mathbf{F}) &= D\boldsymbol{\varphi} - \mathbf{F} = \mathbf{0} \\ \mathbf{g}^S(\mathbf{F},\mathbf{C}) &= \frac{1}{2}(\mathbf{F}^{\mathrm{T}}\mathbf{F} - \mathbf{C}) = \mathbf{0} \end{aligned} \tag{15}$$

Next to the motion $\boldsymbol{\varphi}$ and velocity field $\mathbf{V}$, the independent quantities are the deformation gradient $\mathbf{F} \in \mathcal{M}$, the first Piola-Kirchhoff stress tensor $\mathbf{P} \in \mathcal{M}$, the right Cauchy-Green deformations tensor $\mathbf{C} \in \mathcal{M}$ and the second Piola-Kirchoff stress tensor $\mathbf{S} \in \mathcal{M}$. The stored energy function $W(\mathbf{C})$ depends on $\mathbf{C}$ only. Note that the stress fields $\mathbf{P}$ and $\mathbf{S}$ play the role of Lagrange multipliers for the enforcement of the algebraic constraints in (15). With the condition of stationarity subjected to the end-point conditions, the variational principle in (14) yields the Euler-Lagrange equations. We obtain the stationarity of (14) step-by-step for each independent fields, where the directional derivative is defined by

$$\delta_\bullet S_{\mathrm{HW}} = D_\bullet S_{\mathrm{HW}}(\delta\bullet) \tag{16}$$

For the variation of the velocity field follows

$$\delta_V S_{\mathrm{HW}} = \delta_V \int_{t_0}^{t_e} \int_{\mathcal{B}} \big(\rho_0\,\mathbf{V}\cdot\dot{\boldsymbol{\varphi}} - \frac{1}{2}\rho_0\,\mathbf{V}\cdot\mathbf{V}\big)\,\mathrm{d}V\,\mathrm{d}t = \int_{t_0}^{t_e} \int_{\mathcal{B}} \delta V \cdot \big(\dot{\boldsymbol{\varphi}} - \mathbf{V}\big)\rho_0\,\mathrm{d}V\,\mathrm{d}t \tag{17}$$

The variation of the motion is given by

$$\delta_\varphi S_{\mathrm{HW}} = \delta_\varphi \int_{t_0}^{t_e} \int_{\mathcal{B}} \big(\mathbf{V}\cdot\dot{\boldsymbol{\varphi}}\,\rho_0 - \mathbf{P} : \mathbf{g}^P(\boldsymbol{\varphi},\mathbf{F})\,\mathrm{d}V - V_{\mathrm{ext}}(\boldsymbol{\varphi})\big)\,\mathrm{d}t \tag{18}$$

$$= -\int_{t_0}^{t_e} \int_{\mathcal{B}} \big(\big(\delta\boldsymbol{\varphi}\,\rho_0\cdot\dot{\mathbf{V}} - \mathbf{P} : D\delta\boldsymbol{\varphi}\big)\,\mathrm{d}V - \delta V_{\mathrm{ext}}(\boldsymbol{\varphi})\big)\,\mathrm{d}t + \int_{\mathcal{B}} \big[\mathbf{V}\cdot\delta\boldsymbol{\varphi}\big]_{t_0}^{t_e}\,\mathrm{d}V \tag{19}$$

where we consider

$$\int_{t_0}^{t_e} \int_{\mathcal{B}} \mathbf{V} \cdot \frac{\mathrm{d}}{\mathrm{d}t} \delta\boldsymbol{\varphi}\, \rho_0 \,\mathrm{d}V \,\mathrm{d}t = -\int_{t_0}^{t_e} \int_{\mathcal{B}} \delta\boldsymbol{\varphi} \cdot \rho_0 \,\dot{\mathbf{V}} \,\mathrm{d}V \,\mathrm{d}t + \int_{\mathcal{B}} \left[\mathbf{V} \cdot \delta\boldsymbol{\varphi}\right]_{t_0}^{t_e} \mathrm{d}V \tag{20}$$

The last term vanishes, because $\delta\boldsymbol{\varphi}(t_0) = 0$ and $\delta\boldsymbol{\varphi}(t_e) = 0$. Next, we obtain the variation with respect to the deformation gradient as

$$\begin{aligned} \delta_F S_{\mathrm{HW}} &= \delta_F \int_{t_0}^{t_e} \int_{\mathcal{B}} \left(\mathbf{P} : \mathbf{g}^P(\boldsymbol{\varphi}, \mathbf{F}) + \mathbf{S} : \mathbf{g}^S(\mathbf{F}, \mathbf{C})\right) \mathrm{d}V \,\mathrm{d}t \\ &= \int_{t_0}^{t_e} \int_{\mathcal{B}} \left(\mathbf{P} : (-\delta\mathbf{F}) + \mathbf{S} : \frac{1}{2}(\delta\mathbf{F}^{\mathrm{T}}\,\mathbf{F} + \mathbf{F}^{\mathrm{T}}\delta\mathbf{F})\right) \mathrm{d}V \,\mathrm{d}t \\ &= \int_{t_0}^{t_e} \int_{\mathcal{B}} \delta\mathbf{F} : (-\mathbf{P} + \mathbf{F}\,\mathbf{S}) \,\mathrm{d}V \,\mathrm{d}t \end{aligned} \tag{21}$$

The variation with respect to the right Cauchy-Green deformation tensor leads to

$$\begin{aligned} \delta_C S_{\mathrm{HW}} &= -\delta_C \int_{t_0}^{t_e} \int_{\mathcal{B}} \left(\mathbf{S} : \mathbf{g}^S(\mathbf{F}, \mathbf{C}) + W(\mathbf{C})\right) \mathrm{d}V \,\mathrm{d}t \\ &= -\int_{t_0}^{t_e} \int_{\mathcal{B}} \left(DW(\mathbf{C}) : \delta\mathbf{C} - \frac{1}{2}\mathbf{S} : \delta\mathbf{C}\right) \mathrm{d}V \,\mathrm{d}t \\ &= -\int_{t_0}^{t_e} \int_{\mathcal{B}} \delta\mathbf{C} : \left(DW(\mathbf{C}) - \frac{1}{2}\mathbf{S}\right) \mathrm{d}V \,\mathrm{d}t \end{aligned} \tag{22}$$

For the sake of completeness, the variation with respect to the stress tensors are given by

$$\begin{aligned} \delta_P S_{\mathrm{HW}} &= \delta_P \int_{t_0}^{t_e} \int_{\mathcal{B}} \mathbf{P} : \mathbf{g}^P(\boldsymbol{\varphi}, \mathbf{F}) \,\mathrm{d}V \,\mathrm{d}t = \int_{t_0}^{t_e} \int_{\mathcal{B}} \delta\mathbf{P} : \mathbf{g}^P(\boldsymbol{\varphi}, \mathbf{F}) \,\mathrm{d}V \,\mathrm{d}t \\ \delta_S S_{\mathrm{HW}} &= \delta_S \int_{t_0}^{t_e} \int_{\mathcal{B}} \mathbf{S} : \mathbf{g}^S(\mathbf{F}, \mathbf{C}) \,\mathrm{d}V \,\mathrm{d}t = \int_{t_0}^{t_e} \int_{\mathcal{B}} \delta\mathbf{S} : \mathbf{g}^S(\mathbf{F}, \mathbf{C}) \,\mathrm{d}V \,\mathrm{d}t \end{aligned} \tag{23}$$

The variations can also be written in the form of

$$\begin{aligned}\delta S_{\mathrm{HW}}(\boldsymbol{\varphi},\mathbf{V},\mathbf{F},\mathbf{C},\mathbf{P},\mathbf{S}) = &-\int_{t_0}^{t_e}\int_{\mathcal{B}}\left(\rho_0\,(\dot{\mathbf{V}}-\bar{\mathbf{b}})\cdot\delta\boldsymbol{\varphi}+\mathbf{P}:D\delta\boldsymbol{\varphi}\right)\mathrm{d}V\,\mathrm{d}t\\ &+\int_{t_0}^{t_e}\int_{\mathcal{B}}(\dot{\boldsymbol{\varphi}}-\mathbf{V})\cdot\rho_0\,\delta\mathbf{V}\,\mathrm{d}V\,\mathrm{d}t\\ &-\int_{t_0}^{t_e}\int_{\mathcal{B}}\left(\delta\mathbf{P}:\mathbf{g}^P(\boldsymbol{\varphi},\mathbf{F})+\delta\mathbf{S}:\mathbf{g}^S(\mathbf{F},\mathbf{C})\right)\mathrm{d}V\,\mathrm{d}t\\ &+\int_{t_0}^{t_e}\int_{\mathcal{B}}(\mathbf{P}-\mathbf{F}\,\mathbf{S}):\delta\mathbf{F}\,\mathrm{d}V\,\mathrm{d}t\\ &+\int_{t_0}^{t_e}\int_{\mathcal{B}}\left(\frac{1}{2}\,\mathbf{S}-DW(\mathbf{C})\right):\delta\mathbf{C}\,\mathrm{d}V\,\mathrm{d}t=0\end{aligned}\tag{24}$$

where the external potential energy includes the body forces only. This procedure yields the corresponding Euler-Lagrange equations which can be written as

$$\begin{aligned}\int_{\mathcal{B}}\delta\mathbf{V}\cdot\left(\dot{\boldsymbol{\varphi}}-\mathbf{V}\right)\rho_0\,\mathrm{d}V&=0\\ \int_{\mathcal{B}}\left(\delta\boldsymbol{\varphi}\cdot\rho_0\,(\dot{\mathbf{V}}-\bar{\mathbf{b}})+\mathbf{P}:D\delta\boldsymbol{\varphi}\right)\mathrm{d}V&=0\\ \int_{\mathcal{B}}\delta\mathbf{F}:\left(\mathbf{P}-\mathbf{F}\,\mathbf{S}\right)\mathrm{d}V&=0\\ \int_{\mathcal{B}}\delta\mathbf{C}:\left(\mathbf{S}-2\,DW(\mathbf{C})\right)\mathrm{d}V&=0\\ \int_{\mathcal{B}}\delta\mathbf{P}:\left(D\boldsymbol{\varphi}-\mathbf{F}\right)\mathrm{d}V&=0\\ \int_{\mathcal{B}}\delta\mathbf{S}:\left(\frac{1}{2}(\mathbf{F}^{\mathrm{T}}\mathbf{F}-\mathbf{C})\right)\mathrm{d}V&=0\end{aligned}\tag{25}$$

for all admissible variations $\delta\boldsymbol{\varphi}\in\mathcal{V},\delta\mathbf{V}\in\mathcal{V},\delta\mathbf{F}\in\mathcal{M},\delta\mathbf{P}\in\mathcal{M},\delta\mathbf{C}\in\mathcal{M}$ and $\delta\mathbf{S}\in\mathcal{M}$. The aforementioned variational equations are supplemented by the initial conditions $\boldsymbol{\varphi}\big|_{t=t_0}=\boldsymbol{\varphi}_0$, $\mathbf{V}\big|_{t=t_0}=\mathbf{V}_0$ and the consistent initial conditions $\mathbf{F}\big|_{t=t_0}=\mathbf{F}_0$, $\mathbf{P}\big|_{t=t_0}=\mathbf{P}_0$, $\mathbf{C}\big|_{t=t_0}=\mathbf{C}_0$ and $\mathbf{S}\big|_{t=t_0}=\mathbf{S}_0$. Differentiating $(25)_{5,6}$ with respect to time, we obtain

$$\begin{aligned}\frac{\mathrm{d}}{\mathrm{d}t}\int_{\mathcal{B}}\delta\mathbf{P}:\mathbf{g}^P(\boldsymbol{\varphi},\mathbf{F})\,\mathrm{d}V&=\int_{\mathcal{B}}\delta\mathbf{P}:\frac{\mathrm{d}}{\mathrm{d}t}\mathbf{g}^P(\boldsymbol{\varphi},\mathbf{F})\,\mathrm{d}V=0\\ \frac{\mathrm{d}}{\mathrm{d}t}\int_{\mathcal{B}}\delta\mathbf{S}:\mathbf{g}^S(\mathbf{F},\mathbf{C})\,\mathrm{d}V&=\int_{\mathcal{B}}\delta\mathbf{S}:\frac{\mathrm{d}}{\mathrm{d}t}\mathbf{g}^S(\mathbf{F},\mathbf{C})\,\mathrm{d}V=0\end{aligned}\tag{26}$$

Thus the consistency conditions of the mechanical system are defined by

$$\begin{aligned} \int_{\mathcal{B}} \delta\mathbf{P} : \left(D\dot{\boldsymbol{\varphi}} - \dot{\mathbf{F}}\right) \mathrm{d}V = 0 \\ \int_{\mathcal{B}} \delta\mathbf{S} : \left(\dot{\mathbf{F}}^{\mathrm{T}}\mathbf{F} - \frac{1}{2}\dot{\mathbf{C}}\right) \mathrm{d}V = 0 \end{aligned} \tag{27}$$

Equation (25) along with initial conditions define the weak form of the initial-boundary value problem (IBVP) governing the motion of the considered body. The present IBVP determines solutions $(\boldsymbol{\varphi}, \mathbf{V}, \mathbf{F}, \mathbf{P}, \mathbf{C}, \mathbf{S}) : [t_0, t_e] \mapsto \mathcal{U} \times \mathcal{V} \times \mathcal{M} \times \mathcal{M} \times \mathcal{M} \times \mathcal{M} \mapsto \mathbb{R}$.

2.3 Balance laws of the continuum

In this section we summarize the important conservation laws in the continuous form which should be preserved in the time and space discrete form. Especially if the investigated problem satisfied specific symmetry conditions, the total linear momentum, $\mathbf{L}(\mathbf{V})$, the total angular momentum, $\mathbf{J}(\boldsymbol{\varphi}, \mathbf{V})$, and the total mechanical energy, $E(\boldsymbol{\varphi}, \mathbf{V}, \mathbf{C})$, are first integrals of the motion. The quantities of interest are defined by

$$\begin{aligned} \mathbf{L}(\mathbf{V}) &= \int_{\mathcal{B}} \rho_0 \, \mathbf{V} \, \mathrm{d}V \\ \mathbf{J}(\boldsymbol{\varphi}, \mathbf{V}) &= \int_{\mathcal{B}} \rho_0 \, \boldsymbol{\varphi} \times \mathbf{V} \, \mathrm{d}V \\ E(\boldsymbol{\varphi}, \mathbf{V}, \mathbf{C}) &= \int_{\mathcal{B}} \left(\frac{1}{2}\, \mathbf{V} \cdot \rho_0 \, \mathbf{V} + W(\mathbf{C})\right) \mathrm{d}V + V_{\mathrm{ext}}(\boldsymbol{\varphi}) \end{aligned} \tag{28}$$

Alternatively, the total mechanical energy can be written in the form

$$E(\boldsymbol{\varphi}, \mathbf{V}, \mathbf{C}) = T(\mathbf{V}) + V_{\mathrm{int}}(\boldsymbol{\varphi}, \mathbf{V}, \mathbf{C}) + V_{\mathrm{ext}}(\boldsymbol{\varphi}) \tag{29}$$

where use has been made of (10), (12) and (13).

2.3.1 Balance of energy

At first we proof the balance of energy by choosing $\delta\mathbf{V} = \dot{\mathbf{V}}$ in $(25)_1$ to obtain

$$\int_{\mathcal{B}} \dot{\boldsymbol{\varphi}} \cdot \dot{\mathbf{V}} \, \rho_0 \, dV = \int_{\mathcal{B}} \mathbf{V} \cdot \dot{\mathbf{V}} \, \rho_0 \, dV = \frac{\mathrm{d}}{\mathrm{d}t} \int_{\mathcal{B}} \frac{1}{2} \mathbf{V} \cdot \mathbf{V} \, \rho_0 \, \mathrm{d}V \tag{30}$$

Next, choose $\delta\boldsymbol{\varphi} = \dot{\boldsymbol{\varphi}}$ in $(25)_2$ and along with (30) we get

$$\begin{aligned} &\int_{\mathcal{B}} \left(\dot{\boldsymbol{\varphi}} \cdot \rho_0 \left(\dot{\mathbf{V}} - \bar{\mathbf{b}}\right) + D\dot{\boldsymbol{\varphi}} : \mathbf{P}\right) \mathrm{d}V \\ &= \int_{\mathcal{B}} \mathbf{V} \cdot \rho_0 \, \dot{\mathbf{V}} \, \mathrm{d}V - \int_{\mathcal{B}} \mathbf{V} \cdot \rho_0 \, \bar{\mathbf{b}} \, \mathrm{d}V + \int_{\mathcal{B}} D\dot{\boldsymbol{\varphi}} : P \, \mathrm{d}V \\ &= \int_{\mathcal{B}} \frac{1}{2} \frac{\mathrm{d}}{\mathrm{d}t} \left(\rho_0 \, \mathbf{V} \cdot \mathbf{V}\right) \mathrm{d}V - P_{\mathrm{ext}} + \int_{\mathcal{B}} D\dot{\boldsymbol{\varphi}} : \mathbf{P} \, \mathrm{d}V = 0 \end{aligned} \tag{31}$$

The external power can be evaluated by choosing $\delta\mathbf{V} = \bar{\mathbf{b}}$ in $(25)_1$, so that

$$\int_{\mathcal{B}} \bar{\mathbf{b}} \cdot \dot{\boldsymbol{\varphi}}\, \rho_0\, dV = \int_{\mathcal{B}} \bar{\mathbf{b}} \cdot \mathbf{V}\, \rho_0\, dV = \frac{\mathrm{d}}{\mathrm{d}t} V_{\text{ext}} = P_{\text{ext}} \tag{32}$$

Subsequently we set $\delta\mathbf{P} = \mathbf{P}$ in $(27)_1$ to obtain

$$\int_{\mathcal{B}} \mathbf{P} : D\dot{\boldsymbol{\varphi}}\, \mathrm{d}V = \int_{\mathcal{B}} \mathbf{P} : \dot{\mathbf{F}}\, \mathrm{d}V \tag{33}$$

Choosing $\delta\mathbf{F} = \dot{\mathbf{F}}$ in $(25)_3$ leads to

$$\int_{\mathcal{B}} \dot{\mathbf{F}} : \mathbf{P}\, \mathrm{d}V = \int_{\mathcal{B}} \dot{\mathbf{F}} : (\mathbf{F}\,\mathbf{S})\, \mathrm{d}V = \int_{\mathcal{B}} \mathbf{S} : \left(\dot{\mathbf{F}}^{\mathrm{T}}\mathbf{F}\right)\, \mathrm{d}V \tag{34}$$

For the next step, set $\delta\mathbf{S} = \mathbf{S}$ in $(27)_2$ to get

$$\int_{\mathcal{B}} \mathbf{S} : \left(\dot{\mathbf{F}}^{\mathrm{T}}\mathbf{F}\right)\, \mathrm{d}V = \int_{\mathcal{B}} \mathbf{S} : \frac{1}{2}\dot{\mathbf{C}}\, \mathrm{d}V \tag{35}$$

Eventually, for the choice of $\delta\mathbf{C} = \dot{\mathbf{C}}$ in $(25)_4$ we obtain the result

$$\int_{\mathcal{B}} \frac{1}{2}\dot{\mathbf{C}} : \mathbf{S}\, \mathrm{d}V = \int_{\mathcal{B}} \dot{\mathbf{C}} : DW(\mathbf{C})\, \mathrm{d}V = \frac{\mathrm{d}}{\mathrm{d}t} \int_{\mathcal{B}} W(\mathbf{C})\, \mathrm{d}V \tag{36}$$

and insert the equations (33)-(36) in (31). Accordingly, the total energy is conserved.

2.3.2 Balance of linear momentum

Define $\delta\boldsymbol{\varphi} = \boldsymbol{\zeta}$, where $\boldsymbol{\zeta} \in \mathbb{R}^3$ is a constant vector, so that $D\boldsymbol{\zeta} = \mathbf{0}$. Note that this corresponds to a rigid translation of the body. Next, with $(25)_2$ we obtain

$$\int_{\mathcal{B}} \boldsymbol{\zeta} \cdot \rho_0 \big(\dot{\mathbf{V}} - \bar{\mathbf{b}}\big)\, \mathrm{d}V = 0 \tag{37}$$

The last equation can be recast in the form

$$\boldsymbol{\zeta} \cdot \frac{\mathrm{d}}{\mathrm{d}t} \int_{\mathcal{B}} \rho_0\, \mathbf{V}\, \mathrm{d}V - \boldsymbol{\zeta} \cdot \mathbf{F}_{\text{ext}} = 0 \tag{38}$$

where

$$\mathbf{F}_{\text{ext}} = \int_{\mathcal{B}} \rho_0\, \bar{\mathbf{b}}\, \mathrm{d}V \tag{39}$$

is the external body force. If we consider $(28)_1$, equation (38) yields

$$\boldsymbol{\zeta} \cdot \big(\dot{\mathbf{L}} - \mathbf{F}_{\text{ext}}\big) = 0 \tag{40}$$

This corresponds to the balance law of linear momentum.

2.3.3 Balance of angular momentum

Next, we choose $\delta\boldsymbol{\varphi} = \boldsymbol{\zeta} \times \boldsymbol{\varphi} = \hat{\boldsymbol{\zeta}}\boldsymbol{\varphi}$ in $(25)_2$. This leads to

$$\begin{aligned} &\int_{\mathcal{B}} \left((\boldsymbol{\zeta} \times \boldsymbol{\varphi}) \cdot \rho_0 \left(\dot{\mathbf{V}} - \bar{\mathbf{b}} \right) + (\hat{\boldsymbol{\zeta}}\, D\boldsymbol{\varphi}) : \mathbf{P} \right) \mathrm{d}V \\ &= \boldsymbol{\zeta} \cdot \Big(\int_{\mathcal{B}} \boldsymbol{\varphi} \times \dot{\mathbf{V}}\, \rho_0 \, \mathrm{d}V - \int_{\mathcal{B}} \boldsymbol{\varphi} \times \bar{\mathbf{b}}\, \rho_0 \, \mathrm{d}V \Big) + \int_{\mathcal{B}} \hat{\boldsymbol{\zeta}}\, D\boldsymbol{\varphi} : \mathbf{P} \, \mathrm{d}V = 0 \end{aligned} \tag{41}$$

where $\boldsymbol{\zeta} \in \mathbb{R}^3$ is a constant. Setting $\delta\mathbf{V} = \boldsymbol{\zeta} \times \mathbf{V}$ in $(25)_1$, it follows that

$$\int_{\mathcal{B}} (\boldsymbol{\zeta} \times \mathbf{V}) \cdot (\dot{\boldsymbol{\varphi}} - \mathbf{V})\, \rho_0 \, \mathrm{d}V = \boldsymbol{\zeta} \cdot \left(\int_{\mathcal{B}} \mathbf{V} \times \dot{\boldsymbol{\varphi}}\, \rho_0 \, \mathrm{d}V - \int_{\mathcal{B}} \mathbf{V} \times \mathbf{V}\, \rho_0 \, \mathrm{d}V \right) = 0 \tag{42}$$

Furthermore, it can be observed that

$$\boldsymbol{\zeta} \cdot \frac{\mathrm{d}}{\mathrm{d}t} \int_{\mathcal{B}} \boldsymbol{\varphi} \times \mathbf{V}\, \rho_0 \, \mathrm{d}V = \boldsymbol{\zeta} \cdot \int_{\mathcal{B}} (\dot{\boldsymbol{\varphi}} \times \mathbf{V} + \boldsymbol{\varphi} \times \dot{\mathbf{V}})\, \rho_0 \, \mathrm{d}V = \boldsymbol{\zeta} \cdot \int_{\mathcal{B}} \boldsymbol{\varphi} \times \dot{\mathbf{V}} \, \mathrm{d}V \tag{43}$$

holds. Then we set $\delta\mathbf{P} = \hat{\boldsymbol{\zeta}}\, \mathbf{P}$ in $(25)_5$ to get

$$\int_{\mathcal{B}} (\hat{\boldsymbol{\zeta}}\, \mathbf{P}) : D\boldsymbol{\varphi} \, \mathrm{d}V = \int_{\mathcal{B}} (\hat{\boldsymbol{\zeta}}\, \mathbf{P}) : \mathbf{F} \, \mathrm{d}V \quad \text{or} \quad \int_{\mathcal{B}} \mathbf{P} : (\hat{\boldsymbol{\zeta}}\, D\boldsymbol{\varphi}) \, \mathrm{d}V = \int_{\mathcal{B}} \mathbf{P} : (\hat{\boldsymbol{\zeta}}\mathbf{F}) \, \mathrm{d}V \tag{44}$$

Eventually, choose $\delta\mathbf{F} = \hat{\boldsymbol{\zeta}}\, \mathbf{F}$ in $(25)_3$ and note that $\hat{\boldsymbol{\zeta}} = -\hat{\boldsymbol{\zeta}}^{\mathrm{T}}$ to obtain

$$\int_{\mathcal{B}} \mathbf{P} : (\hat{\boldsymbol{\zeta}}\, \mathbf{F}) \, \mathrm{d}V = \int_{\mathcal{B}} \hat{\boldsymbol{\zeta}}\, \mathbf{F} : (\mathbf{F}\, \mathbf{S}) \, \mathrm{d}V = \int_{\mathcal{B}} \mathbf{S} : (\mathbf{F}^{\mathrm{T}} \hat{\boldsymbol{\zeta}}\, \mathbf{F}) \, \mathrm{d}V = 0 \tag{45}$$

As a result, we recast equation $(25)_2$ under consideration of (41)-(45) to

$$\boldsymbol{\zeta} \cdot \frac{\mathrm{d}}{\mathrm{d}t} \int_{\mathcal{B}} \boldsymbol{\varphi} \times \mathbf{V} \rho_0 \, \mathrm{d}V - \boldsymbol{\zeta} \cdot \mathbf{M}_{\mathrm{ext}} = 0 \tag{46}$$

Associated with $(28)_2$, it follows

$$\boldsymbol{\zeta} \cdot \left(\dot{\mathbf{J}} - \mathbf{M}_{\mathrm{ext}} \right) = 0 \tag{47}$$

where the external moment $\mathbf{M}_{\mathrm{ext}}$ depends on the body forces only and can be written as

$$\mathbf{M}_{\mathrm{ext}} = \int_{\mathcal{B}} \boldsymbol{\varphi} \times \bar{\mathbf{b}}\, \rho_0 \, \mathrm{d}V \tag{48}$$

Because (47) holds for all $\boldsymbol{\zeta} \in \mathbb{R}^3$, the angular momentum is a conserved quantity if $\mathbf{M}_{\mathrm{ext}} = \mathbf{0}$.

3 Discretization in time

We next focus on the design of a structure-preserving discretization in time of the underlying variational formulation (25). In particular, we aim at time-stepping scheme which inherit the important conservation properties described above.

3.1 Energy-momentum consistent time-stepping scheme

Consider a representative time interval $[t_0, t_e]$ with time-step size $\Delta t = t_{n+1} - t_n$, given state space coordinates $(\boldsymbol{\varphi}_n, \mathbf{V}_n) \in \mathbb{R}^3 \times \mathbb{R}^3$, consistent deformation states $\mathbf{F}_n \in \mathcal{M}$, $\mathbf{C}_n \in \mathcal{M}$ and stresses $\mathbf{P}_n \in \mathcal{M}$, $\mathbf{S}_n \in \mathcal{M}$ at t_n. We show below, that a mid-point type discretization of the IBVP results in an energy-momentum scheme, which inherits the important balance laws from the continuous case. The energy-momentum consistent scheme may be formulated as

$$\begin{aligned}
\int_{\mathcal{B}} \delta\mathbf{V} \cdot \frac{1}{\Delta t} \left(\boldsymbol{\varphi}_{n+1} - \boldsymbol{\varphi}_n \right) \rho_0 \, \mathrm{d}V &= \int_{\mathcal{B}} \delta\mathbf{V} \cdot \mathbf{V}_{n+\frac{1}{2}} \, \rho_0 \, \mathrm{d}V \\
\int_{\mathcal{B}} \delta\boldsymbol{\varphi} \cdot \frac{1}{\Delta t} \, \rho_0 \left(\mathbf{V}_{n+1} - \mathbf{V}_n \right) \mathrm{d}V &= - \int_{\mathcal{B}} \mathbf{P}_{n+1} : D\delta\boldsymbol{\varphi} \, \mathrm{d}V + \int_{\mathcal{B}} \delta\boldsymbol{\varphi} \cdot \rho_0 \, \bar{\mathbf{b}} \, \mathrm{d}V \\
\int_{\mathcal{B}} \delta\mathbf{F} : \Big(\mathbf{P}_{n+1} - \mathbf{F}_{n+\frac{1}{2}} \, \mathbf{S}_{n+1} \Big) \, \mathrm{d}V &= 0 \\
\int_{\mathcal{B}} \delta\mathbf{C} : \Big(\mathbf{S}_{n+1} - 2 \, DW(\mathbf{C}_{n+\frac{1}{2}}) \Big) \, \mathrm{d}V &= 0 \\
\int_{\mathcal{B}} \delta\mathbf{P} : \left(D\boldsymbol{\varphi}_{n+1} - \mathbf{F}_{n+1} \right) \mathrm{d}V &= 0 \\
\int_{\mathcal{B}} \delta\mathbf{S} : \left(\frac{1}{2} \Big(\mathbf{F}_{n+1}^{\mathrm{T}} \mathbf{F}_{n+1} - \mathbf{C}_{n+1} \Big) \right) \mathrm{d}V &= 0
\end{aligned} \tag{49}$$

for all $\delta\boldsymbol{\varphi}, \delta\mathbf{V} \in \mathcal{V}$, $\delta\mathbf{F} \in \mathcal{M}$, $\delta\mathbf{P} \in \mathcal{M}$, $\delta\mathbf{C} \in \mathcal{M}$, $\delta\mathbf{S} \in \mathcal{M}$. The mid-point value of the quantity $(\bullet)$ is evaluated by $(\bullet) = \frac{1}{2}((\bullet)_n + (\bullet)_{n+1})$. Then the energy-momentum consistent scheme in (49) determines the state-space coordinates $(\boldsymbol{\varphi}_{n+1}, \mathbf{V}_{n+1}) \in \mathbb{R}^3 \times \mathbb{R}^3$, consistent deformation states $\mathbf{F}_{n+1} \in \mathcal{M}$, $\mathbf{C}_{n+1} \in \mathcal{M}$ at t_{n+1} and the consistent stresses $\mathbf{P}_{n+1} \in \mathcal{M}$, $\mathbf{S}_{n+1} \in \mathcal{M}$ in the time interval $[t_0, t_e]$. As mentioned above, our algorithm is based on the mid-point discretization, however, the constraints are evaluated at the end of each time step. The time discrete counterpart of the condition of consistency $(27)_1$ is given by

$$\int_{\mathcal{B}} \delta\mathbf{P} : \left(D\boldsymbol{\varphi}_{n+1} - D\boldsymbol{\varphi}_n \right) \mathrm{d}V = \int_{\mathcal{B}} \delta\mathbf{P} : \left(\mathbf{F}_{n+1} - \mathbf{F}_n \right) \mathrm{d}V \tag{50}$$

and $(27)_2$ can be written in the time-discrete form as

$$\begin{aligned} &\int_{\mathcal{B}} \delta\mathbf{S} : \left(\frac{1}{2}\Big(\mathbf{F}_{n+1}^{\mathrm{T}}\mathbf{F}_{n+1} - \mathbf{C}_{n+1} - \Big(\mathbf{F}_{n}^{\mathrm{T}}\mathbf{F}_{n} - \mathbf{C}_{n} \Big) \Big) \right) \mathrm{d}V \\ =& \int_{\mathcal{B}} \delta\mathbf{S} : \left(\mathbf{F}_{n+\frac{1}{2}}^{\mathrm{T}} \left(\mathbf{F}_{n+1} - \mathbf{F}_{n} \right) - \frac{1}{2}(\mathbf{C}_{n+1} - \mathbf{C}_{n}) \right) \mathrm{d}V \\ =& \quad 0 \end{aligned} \tag{51}$$

The specific temporal discretization of the IBVP results in the algorithm (49) which defines an energy momentum consistent scheme. Consequently the physical quantities in (28) are consistently approximated independent of the time-step size.

Remark 1 *In the present work we focus on St. Venant-Kirchhoff type material models. It can be easily verified, that*

$$DW(\mathbf{C}_{n+\frac{1}{2}}) : (\mathbf{C}_{n+1} - \mathbf{C}_{n}) = W(\mathbf{C}_{n+1}) - W(\mathbf{C}_{n}) \tag{52}$$

In case of material models suitable for finite elasticity, $DW(\mathbf{C}_{n+\frac{1}{2}})$ *in* (49) *has to be replaced by an appropriate discrete derivative* $\bar{D}W(\mathbf{C}_{n+\frac{1}{2}})$ *in the sense of Gonzalez [10, 11].*

3.2 Discrete balance laws

In this section, we show that the EMC scheme exactly inherited the significant consistency (and conservation) properties from the underlying continuous formulation presented in section 2.3.

3.2.1 Discrete conservation of energy

We start with the proof of the energy conservation by choosing $\delta\mathbf{V} = \mathbf{V}_{n+1} - \mathbf{V}_{n}$ in $(49)_1$ to obtain

$$\begin{aligned} \int_{\mathcal{B}} (\mathbf{V}_{n+1} - \mathbf{V}_{n}) \cdot \frac{1}{\Delta t}\, \rho_0 \left(\boldsymbol{\varphi}_{n+1} - \boldsymbol{\varphi}_{n} \right) &= \int_{\mathcal{B}} (\mathbf{V}_{n+1} - \mathbf{V}_{n}) \cdot \mathbf{V}_{n+\frac{1}{2}}\, \rho_0 \, \mathrm{d}V \\ &= \frac{1}{2} \int_{\mathcal{B}} (\mathbf{V}_{n+1} \cdot \mathbf{V}_{n+1} - \mathbf{V}_{n} \cdot \mathbf{V}_{n})\, \rho_0 \, \mathrm{d}V \\ &= T(\mathbf{V}_{n+1}) - T(\mathbf{V}_{n}) \end{aligned} \tag{53}$$

Next we choose $\delta\boldsymbol{\varphi} = \boldsymbol{\varphi}_{n+1} - \boldsymbol{\varphi}_{n}$ in $(49)_2$ and observe that

$$\begin{aligned} &\int_{\mathcal{B}} (\boldsymbol{\varphi}_{n+1} - \boldsymbol{\varphi}_{n}) \cdot \frac{1}{\Delta t}\, \rho_0 \left(\mathbf{V}_{n+1} - \mathbf{V}_{n} \right) \mathrm{d}V \\ &\qquad = - \int_{\mathcal{B}} \mathbf{P}_{n+1} : (D\boldsymbol{\varphi}_{n+1} - D\boldsymbol{\varphi}_{n})\, \mathrm{d}V + \int_{\mathcal{B}} (\boldsymbol{\varphi}_{n+1} - \boldsymbol{\varphi}_{n}) \cdot \rho_0\, \bar{\mathbf{b}}\, \mathrm{d}V \end{aligned} \tag{54}$$

We notice, that for the discrete form of the external potential energy

$$\int_{\mathcal{B}} (\boldsymbol{\varphi}_{n+1} - \boldsymbol{\varphi}_n) \cdot \rho_0 \, \bar{\mathbf{b}} \, \mathrm{d}V = V_{\mathrm{ext}}(\boldsymbol{\varphi}_{n+1}) - V_{\mathrm{ext}}(\boldsymbol{\varphi}_n) \tag{55}$$

holds. Then we use $\delta\mathbf{P} = \mathbf{P}_{n+1}$ in (50) to get

$$\int_{\mathcal{B}} \mathbf{P}_{n+1} : (D\boldsymbol{\varphi}_{n+1} - D\boldsymbol{\varphi}_n) \, \mathrm{d}V = \int_{\mathcal{B}} \mathbf{P}_{n+1} : (\mathbf{F}_{n+1} - \mathbf{F}_n) \, \mathrm{d}V \tag{56}$$

After that, set $\delta\mathbf{F} = \mathbf{F}_{n+1} - \mathbf{F}_n$ in $(49)_3$ to obtain

$$\begin{aligned} \int_{\mathcal{B}} \mathbf{P}_{n+1} : (\mathbf{F}_{n+1} - \mathbf{F}_n) \, \mathrm{d}V &= \int_{\mathcal{B}} (\mathbf{F}_{n+1} - \mathbf{F}_n) : \mathbf{F}_{n+\frac{1}{2}} \, \mathbf{S}_{n+1} \, \mathrm{d}V \\ &= \int_{\mathcal{B}} \mathbf{S}_{n+1} : \mathbf{F}^{\mathrm{T}}_{n+\frac{1}{2}} \, (\mathbf{F}_{n+1} - \mathbf{F}_n) \, \mathrm{d}V \end{aligned} \tag{57}$$

For the variation of the second Piola-Kichhoff stress tensor we choose $\delta\mathbf{S} = \mathbf{S}_{n+1}$ in (51) and as a result, we get

$$\int_{\mathcal{B}} \mathbf{S}_{n+1} : \mathbf{F}^{\mathrm{T}}_{n+\frac{1}{2}} \, (\mathbf{F}_{n+1} - \mathbf{F}_n) \, \mathrm{d}V = \int_{\mathcal{B}} \mathbf{S}_{n+1} : \frac{1}{2} (\mathbf{C}_{n+1} - \mathbf{C}_n) \, \mathrm{d}V \tag{58}$$

Accordingly, choosing $\delta\mathbf{C} = \mathbf{C}_{n+1} - \mathbf{C}_n$ in $(49)_4$ leads to

$$\int_{\mathcal{B}} \mathbf{S}_{n+1} : \frac{1}{2} (\mathbf{C}_{n+1} - \mathbf{C}_n) \, \mathrm{d}V = \int_{\mathcal{B}} DW(\mathbf{C}_{n+\frac{1}{2}}) : (\mathbf{C}_{n+1} - \mathbf{C}_n) \, \mathrm{d}V \tag{59}$$

As a result, for (54) along with (53), (55) and (56)-(59) we obtain

$$T(\mathbf{V}_{n+1}) + V_{\mathrm{int}}(\mathbf{C}_{n+1}) + V_{\mathrm{ext}}(\boldsymbol{\varphi}_{n+1}) = T(\mathbf{V}_n) + V_{\mathrm{int}}(\mathbf{C}_n) + V_{\mathrm{ext}}(\boldsymbol{\varphi}_n) \tag{60}$$

Thus, the EMC scheme reproduces the total mechanical energy exactly, independent of the time-step size. Note that in the last equation the relationship (52) has been used.

3.2.2 Discrete balance of linear momentum

We next choose $\delta\boldsymbol{\varphi} = \boldsymbol{\zeta}$ where $\boldsymbol{\zeta} \in \mathbb{R}^3$ is constant so that, $D\boldsymbol{\zeta} = \mathbf{0}$. Now, its straightforward to show that $(49)_2$ yields the result

$$\int_{\mathcal{B}} \boldsymbol{\zeta} \cdot \rho_0 \left(\frac{1}{\Delta t} (\mathbf{V}_{n+1} - \mathbf{V}_n) - \bar{\mathbf{b}} \right) \mathrm{d}V = 0 \tag{61}$$

which we can recast by $(28)_1$ in the form

$$\boldsymbol{\zeta} \cdot \left(\mathbf{L}(\mathbf{V}_{n+1}) - L(\mathbf{V}_n) + \Delta t \, \mathbf{F}_{\mathrm{ext}} \Big|_{n+\alpha} \right) = 0 \tag{62}$$

where

$$\mathbf{F}_{\text{ext}}\Big|_{n+\alpha} = \int_{\mathcal{B}} \rho_0 \, \bar{\mathbf{b}} \, \mathrm{d}V \tag{63}$$

are the external body forces in the time interval $[t_n, t_{n+1}]$. This is the discrete version of the linear momentum balance corresponding to $(28)_1$. Hence, the linear momentum is a conserved quantity in $[t_n, t_{n+1}]$ for any $\alpha \in [0, 1]$ if no external forces are acting on the body.

3.2.3 Discrete balance of angular momentum

We now choose $\delta\boldsymbol{\varphi} = (\boldsymbol{\zeta} \times \boldsymbol{\varphi}_{n+\frac{1}{2}}) = \hat{\boldsymbol{\zeta}}\, \boldsymbol{\varphi}_{n+\frac{1}{2}}$ in $(49)_2$. We conclude that

$$\begin{aligned}
&\int_{\mathcal{B}} (\boldsymbol{\zeta} \times \boldsymbol{\varphi}_{n+\frac{1}{2}}) \cdot \frac{1}{\Delta t} \, \rho_0 \, (\mathbf{V}_{n+1} - \mathbf{V}_n) \, \mathrm{d}V \\
&\qquad + \int_{\mathcal{B}} \mathbf{P}_{n+1} : (\hat{\boldsymbol{\zeta}}\, D\boldsymbol{\varphi}_{n+\frac{1}{2}}) \, \mathrm{d}V - \int_{\mathcal{B}} (\boldsymbol{\zeta} \times \boldsymbol{\varphi}_{n+\frac{1}{2}}) \cdot \rho_0 \, \bar{\mathbf{b}} \, \mathrm{d}V \\
&= \boldsymbol{\zeta} \cdot \left(\int_{\mathcal{B}} \boldsymbol{\varphi}_{n+\frac{1}{2}} \times (\mathbf{V}_{n+1} - \mathbf{V}_n) \frac{1}{\Delta t} \, \rho_0 \, \mathrm{d}V - \int_{\mathcal{B}} \boldsymbol{\varphi}_{n+\frac{1}{2}} \times \bar{\mathbf{b}} \, \rho_0 \, \mathrm{d}V \right) \\
&\qquad + \int_{\mathcal{B}} \hat{\boldsymbol{\zeta}}\, \mathbf{P}_{n+1} : D\boldsymbol{\varphi}_{n+\frac{1}{2}} \, \mathrm{d}V \\
&= 0
\end{aligned} \tag{64}$$

Then we choose $\delta\mathbf{P}_{n+1} = \hat{\boldsymbol{\zeta}}\mathbf{P}_{n+1}$ in $(49)_5$ to obtain

$$\int_{\mathcal{B}} (\hat{\boldsymbol{\zeta}}\, \mathbf{P}_{n+1}) : D\boldsymbol{\varphi}_{n+1} \, \mathrm{d}V = \int_{\mathcal{B}} \hat{\boldsymbol{\zeta}}\, \mathbf{P}_{n+1} : \mathbf{F}_{n+1} \, \mathrm{d}V \tag{65}$$

or equally

$$\int_{\mathcal{B}} \mathbf{P}_{n+1} : (\hat{\boldsymbol{\zeta}}\, D\boldsymbol{\varphi}_{n+1}) \, \mathrm{d}V = \int_{\mathcal{B}} \mathbf{P}_{n+1} : (\hat{\boldsymbol{\zeta}}\, \mathbf{F}_{n+1}) \, \mathrm{d}V \tag{66}$$

Similarly, for the constraints at t_n with $\delta\mathbf{P} = \hat{\boldsymbol{\zeta}}\, \mathbf{P}_{n+1}$ we get

$$\int_{\mathcal{B}} \mathbf{P}_{n+1} : (\hat{\boldsymbol{\zeta}}\, D\boldsymbol{\varphi}) \, \mathrm{d}V = \int_{\mathcal{B}} \mathbf{P}_{n+1} (\hat{\boldsymbol{\zeta}}\, \mathbf{F}_n) \, \mathrm{d}V \tag{67}$$

We take the average of the equations from above as $\frac{1}{2}[(66) + (67)]$ to get

$$\begin{aligned}
\int_{\mathcal{B}} \mathbf{P}_{n+1} : (\hat{\boldsymbol{\zeta}}\, D\boldsymbol{\varphi}_{n+\frac{1}{2}}) \, \mathrm{d}V &= \int_{\mathcal{B}} \mathbf{P}_{n+1} : \left(\hat{\boldsymbol{\zeta}}\, \frac{1}{2} (\mathbf{F}_n + \mathbf{F}_{n+1}) \right) \mathrm{d}V \\
&= \int_{\mathcal{B}} \mathbf{P}_{n+1} : \left(\hat{\boldsymbol{\zeta}}\, \mathbf{F}_{n+\frac{1}{2}} \right) \mathrm{d}V
\end{aligned} \tag{68}$$

Now let $\delta\mathbf{F} = \hat{\boldsymbol{\zeta}}\,\frac{1}{2}(\mathbf{F_n} + \mathbf{F}_{n+1})$ in $(49)_3$ to verify that

$$\begin{aligned}\int_{\mathcal{B}} \mathbf{P}_{n+1} : \left(\hat{\boldsymbol{\zeta}}\,\frac{1}{2}(\mathbf{F}_n + \mathbf{F}_{n+1})\right) \mathrm{d}V &= \int_{\mathcal{B}} \mathbf{F}_{n+\frac{1}{2}}\,\mathbf{S}_{n+1} : \left(\hat{\boldsymbol{\zeta}}\,\frac{1}{2}(\mathbf{F}_n + \mathbf{F}_{n+1})\right) \mathrm{d}V \\ &= \int_{\mathcal{B}} \mathbf{S}_{n+1} : \mathbf{F}^{\mathrm{T}}_{n+\frac{1}{2}} \left(\hat{\boldsymbol{\zeta}}\,\frac{1}{2}(\mathbf{F}_n + \mathbf{F}_{n+1})\right) \mathrm{d}V \\ &= \quad 0\end{aligned} \tag{69}$$

Consider equation (64) along with (65) - (69) to get:

$$\boldsymbol{\zeta} \cdot \left(\mathbf{J}(\boldsymbol{\varphi}_{\mathbf{n+1}}, \mathbf{V}_{n+1}) - \mathbf{J}(\boldsymbol{\varphi}_n, \mathbf{V}_n) + \Delta t \mathbf{M}_{\mathrm{ext}}\Big|_{n+\frac{1}{2}}\right) = 0 \tag{70}$$

This is the discrete version of the angular momentum balance corresponding to $(28)_2$. Note, that the external moment is evaluated at the mid-point configuration as

$$\mathbf{M}_{\mathrm{ext}}\Big|_{n+\frac{1}{2}} = \int_{\mathcal{B}} \boldsymbol{\varphi}_{n+\frac{1}{2}} \times \rho_0\, \bar{\mathbf{b}}\, \mathrm{d}V \tag{71}$$

4 Discretization in space

In this section, we deal with the finite element method to accomplish a numerical solution for the semi-discrete mechanical system. We start our developments by the approximation of the body in its reference configuration by

$$\mathcal{B} \approx \mathcal{B}^h = \bigcup_{e}^{n_{el}} \Omega_e \tag{72}$$

Accordingly the boundaries are approximated by $\partial\mathcal{B} \approx \partial\mathcal{B}^h = \bigcup_e^{n_{el}} \partial\Omega_e$. Next, we make use of standard isoparametric finite elements for the finite dimensional approximation of $\boldsymbol{\varphi}$, and the velocity $\mathbf{V}$ as

$$\boldsymbol{\varphi}^h(\mathbf{X}, t) = \sum_{A=1}^{n^e_{node}} N_A(\mathbf{X})\, \boldsymbol{\varphi}^A \quad \text{and} \quad \mathbf{V}^h(\mathbf{X}, t) = \sum_{A=1}^{n^e_{node}} N_A(\mathbf{X})\, \mathbf{V}^A \tag{73}$$

where n^e_{node} are the nodes of the element Ω_e and $N_A(\mathbf{X}) : \mathcal{B} \to \mathbb{R}$ are the standard isoparametric shape functions associated with node A. Note that the nodal vectors of an element are denoted by $\boldsymbol{\varphi}^A \in \mathbb{R}^3$ and $\mathbf{V}^A \in \mathbb{R}^3$. In the present work we deal with trilinear shapefunctions with the property that $N_A(\mathbf{X}_B) = \delta^B_A$. The finite element spaces are given due to the approximation in (73) by $\mathcal{U}^h \subset \mathcal{U}$ and $\mathcal{V}^h \subset \mathcal{V}$.

By inserting the spatial interpolations in (6), the approximation of the deformation gradient is given by

$$\widetilde{\mathbf{F}} = \frac{\partial \boldsymbol{\varphi}(\mathbf{X}, t)}{\partial \mathbf{X}} = \sum_{A=1}^{n^e_{node}} \boldsymbol{\varphi}^A \otimes \nabla_X N_A(\mathbf{X}) \tag{74}$$

Next, we define the kinetic energy of an element by (10) with (73) as

$$T = \frac{1}{2} \sum_{A,B=1}^{n^e_{node}} \mathbf{V}^A \cdot \mathbf{M}^{AB}_{\rho} \mathbf{V}^B \quad \text{with} \quad \mathbf{M}^{AB}_{\rho} = \int_{\Omega_e} \rho_0 \, N_A N_B \, \mathrm{d}V \, \mathbf{I} \tag{75}$$

where $\mathbf{I} \in \mathbb{R}^{3\times3}$ represents the identity matrix. The external potential energy, given in (12) can be expresses in the discrete form as

$$V_{ext} = -\sum_{A=1}^{n^e_{node}} \boldsymbol{\varphi}^A \cdot \mathbf{F}^A_{ext} \quad \text{where} \quad \mathbf{F}^A_{ext} = \int_{\Omega_e} N^A \, \bar{\mathbf{b}} \, \mathrm{d}V + \int_{\partial\Omega_e} N^A \, \bar{\mathbf{t}} \, \mathrm{d}A \tag{76}$$

where $\mathbf{F}^A_{ext} \in \mathbb{R}^3$ denotes the external forces associated with node A.

4.1 Mixed approximation

In the present work the discretization of the mixed quantities follows the approach by Kasper & Taylor [15]. They developed a mixed-enhanced finite element with mixed stress field $\mathbf{P}$ and an mixed-enhanced strain field $\mathbf{F}$. The other independent quantities, namely the right Cauchy-Green deformation tensor $\mathbf{C}$ and the second Piola-Kirchhoff stress tensor $\mathbf{S}$ are calculated by the constraints given in $(14)_{5,6}$. Accordingly, we are very flexible in the design of an EMC algorithm as we show below.

Consider a mixed stress and strain field, formulated in the isoparametric space and then use a standard transform to define the approximations in the physical space. The approximation of the deformation gradient is defined by

$$\mathbf{F} = \boldsymbol{\gamma}_0 + \frac{1}{j(\boldsymbol{\xi})} \mathbf{F}_0 \, \mathbf{T} [\boldsymbol{\mathcal{E}}_1(\boldsymbol{\xi}, \boldsymbol{\gamma}) - \boldsymbol{\mathcal{E}}_2(\boldsymbol{\xi}, \boldsymbol{\alpha})] \mathbf{T}^{\mathrm{T}} \tag{77}$$

For the approximation of the first Piola-Kirchhoff stress tensor we obtain

$$\mathbf{P} = \boldsymbol{\beta}_0 + \mathbf{F}_0^{-\mathrm{T}} \, \mathbf{T}^{-\mathrm{T}} [\boldsymbol{\mathcal{E}}_1(\boldsymbol{\xi}, \boldsymbol{\beta})] \mathbf{T}^{-1} \tag{78}$$

where $\mathbf{F} \in \mathcal{M}^h$, $\mathbf{P} \in \mathcal{M}^h$ with $\mathcal{M}^h \subset \mathcal{M}$. On element level we have 26 additional local parameters for the mixed stress, where $\boldsymbol{\beta}_0 \in \mathbb{R}^{3\times3}$ ensures constant stress states within the element and $\boldsymbol{\beta} \in \mathbb{R}^{15}$ reflects the varying stress field. In contrast, the mixed-enhanced deformation gradient is approximated by 35 local parameters. Similar to the mixed stress we have $\boldsymbol{\gamma}_0 \in \mathbb{R}^{3\times3}$ parameters for the constant part and $\boldsymbol{\gamma} \in \mathbb{R}^{15}$ parameters for the varying part. In addition, the enhanced parameters $\boldsymbol{\alpha} \in \mathbb{R}^9$ were added to improve the element performance. The interpolations $\boldsymbol{\mathcal{E}}_1(\boldsymbol{\xi}, \bullet)$ and $\boldsymbol{\mathcal{E}}_2(\boldsymbol{\xi}, \boldsymbol{\alpha})$ can be found in Appendix A.1. The approximation of the mixed quantities contains $\mathbf{T}$ and $\mathbf{F}_0$ to ensure constant states, minimize the order of quadrature and reduce the sensitivity to

Matrix	i	1	2	3	1	2	1	2	3	3
	j	1	2	3	2	3	3	1	2	1
Vector	i	1	2	3	4	5	6	7	8	9

Table 1: Matrix-vector notation

initially distorted elements. Note that $\mathbf{F}_0$ ensures an objective formulation to a superposed rigid body motion. Theses quantities are evaluated at the center of the element as

$$\mathbf{F}_0 = \mathrm{Grad}\boldsymbol{\varphi}^h\big|_{\xi=0} = \sum_{A=1}^{n^e_{node}} \boldsymbol{\varphi}^A \otimes \nabla_0 N_A(\mathbf{X}) \tag{79}$$

and

$$\mathbf{T} = \mathbf{J}\big|_{\xi=0} \quad \text{where} \quad \mathbf{J} = \mathrm{Grad}_\xi \mathbf{X}^h, \quad j(\boldsymbol{\xi}) = \mathrm{det}\mathbf{J} \tag{80}$$

Remark 2 *Alternatively,* $\mathbf{T}$ *and* $\mathbf{F}_0$ *can be calculated as the average over the element by*

$$\mathbf{T} = \frac{1}{\Omega_e}\int_{\Omega_e} \mathbf{J}(\boldsymbol{\xi})\,\mathrm{d}V, \qquad \mathbf{F}_0 = \frac{1}{\Omega_e}\int_{\Omega_e} \widetilde{\mathbf{F}}\,\mathrm{d}V \tag{81}$$

Note that in the two dimensional case both formulations are identical.

4.2 Efficient formulation and variation

We start this section with an matrix-vector transformation to make use of the linearity of the element parameters. Then we apply the variation of the mixed quantities.

4.2.1 Efficient formulation of the approximations

Since the local parameters are linear within the element, an efficient reformulation is possible. Therefore we may write

$$\begin{aligned}
\widetilde{\mathbf{F}} = \sum_{A=1}^{n^e_{node}} \boldsymbol{\varphi}^A \otimes \nabla_X N_A(\mathbf{X}) \;&\xrightarrow{i,j\to i}\; \widetilde{\mathbf{F}}^{\mathrm{v}} = \mathbf{B}\,\boldsymbol{\varphi}^v \\
\mathbf{F} = \boldsymbol{\gamma}_0 + \frac{1}{j(\boldsymbol{\xi})}\mathbf{F}_0\,\mathbf{T}[\boldsymbol{\mathcal{E}}_1(\boldsymbol{\xi},\boldsymbol{\gamma}) - \boldsymbol{\mathcal{E}}_2(\boldsymbol{\xi},\boldsymbol{\alpha})]\mathbf{T}^{\mathrm{T}} \;&\xrightarrow{i,j\to i}\; \mathbf{F}^{\mathrm{v}} = \boldsymbol{\gamma}_0^v + \mathbf{B}_\gamma(\boldsymbol{\varphi})\,\boldsymbol{\gamma} - \mathbf{B}_\alpha(\boldsymbol{\varphi})\,\boldsymbol{\alpha} \\
\mathbf{P} = \boldsymbol{\beta}_0 + \mathbf{F}_0^{-\mathrm{T}}\,\mathbf{T}^{-\mathrm{T}}[\boldsymbol{\mathcal{E}}_1(\boldsymbol{\xi},\boldsymbol{\beta})]\mathbf{T}^{-1} \;&\xrightarrow{i,j\to i}\; \mathbf{P}^{\mathrm{v}} = \boldsymbol{\beta}_0^v + \mathbf{B}_\beta(\boldsymbol{\varphi})\,\boldsymbol{\beta}
\end{aligned} \tag{82}$$

where the ordering for the matrix-vector notation is given in Table 1. Due to the formulation in (82), the approximations can be written in a vectorial form as $\widetilde{\mathbf{F}}^v \in \mathbb{R}^9, \mathbf{F}^v \in \mathbb{R}^9$

or $\mathbf{P}^v \in \mathbb{R}^9$, respectively. Then we can calculate them along with the element operator-matrices $\mathbf{B} \in \mathbb{R}^{9\times 24}$, $\mathbf{B}_\gamma(\boldsymbol{\varphi}) \in \mathbb{R}^{9\times 15}$, $\mathbf{B}_\alpha(\boldsymbol{\varphi}) \in \mathbb{R}^{9\times 9}$ or $\mathbf{B}_\beta(\boldsymbol{\varphi}) \in \mathbb{R}^{9\times 15}$ and the local element parameters $\boldsymbol{\gamma}_0^v \in \mathbb{R}^9$ and $\boldsymbol{\beta}_0^v \in \mathbb{R}^9$ in the vectorial form. Note, that the nodal vectors are summarized to $\boldsymbol{\varphi}^v = [\boldsymbol{\varphi}^{1\mathrm{T}} ... \boldsymbol{\varphi}^{8\mathrm{T}}]^{\mathrm{T}}$.

4.2.2 Variations

Consider the variations of the equation given in (82) with respect to both the local element parameters and nodal parameters. For the variation to the one mentioned first we obtain

$$\begin{aligned} \delta_{\gamma_0}\mathbf{F}^{\mathrm{v}} &= \delta\boldsymbol{\gamma}_0^v & \qquad \delta_{\beta_0}\mathbf{P}^{\mathrm{v}} &= \delta\boldsymbol{\beta}_0^v \\ \delta_{\gamma}\mathbf{F}^{\mathrm{v}} &= \mathbf{B}_\gamma(\boldsymbol{\varphi})\,\delta\boldsymbol{\gamma}, & \qquad \delta_{\beta}\mathbf{P}^{\mathrm{v}} &= \mathbf{B}_\beta(\boldsymbol{\varphi})\,\delta\boldsymbol{\beta} \\ \delta_{\alpha}\mathbf{F}^{\mathrm{v}} &= -\mathbf{B}_\alpha(\boldsymbol{\varphi})\,\delta\boldsymbol{\alpha} \end{aligned} \tag{83}$$

For the variation with respect to the nodal parameters we get

$$\begin{aligned} \delta_q\widetilde{\mathbf{F}} &= \sum_{A=1}^{n^e_{node}} \delta\boldsymbol{\varphi}^A \otimes \nabla_X N_A(\mathbf{X}) \\ \delta_q\mathbf{F} &= \Big(\sum_{A=1}^{n^e_{node}} \delta\boldsymbol{\varphi}^A \otimes \nabla_0 N_A\Big)\,\mathbf{T}\,(\boldsymbol{\mathcal{E}}_1(\boldsymbol{\xi},\boldsymbol{\gamma}) - \boldsymbol{\mathcal{E}}_2(\boldsymbol{\xi},\boldsymbol{\alpha}))\,\mathbf{T}^{\mathrm{T}} \\ \delta_q\mathbf{P} &= -\mathbf{F}_0^{-\mathrm{T}}\Big(\sum_{A=1}^{n^e_{node}} \delta\boldsymbol{\varphi}^A \otimes \nabla_0 N_A\Big)^{\mathrm{T}}\mathbf{F}_0^{-\mathrm{T}}\,\mathbf{T}^{-\mathrm{T}}\,\boldsymbol{\mathcal{E}}_1(\boldsymbol{\xi},\boldsymbol{\beta})\,\mathbf{T}^{-1} \end{aligned} \tag{84}$$

4.3 Fully discrete system

The present implementation differs from the original approach by Kasper & Taylor since the mixed strain parameters $\boldsymbol{\gamma}_0, \boldsymbol{\gamma}$ are not solved by the nodal parameters directly. Thus, we facilitate the implementation and further improve the clarity of the underlying formulation as we see below. Furthermore, a direct variational stress recovery for post-processing is available. Since a static condensation process is still possible, the number of global unknowns are identical and thus, the computational effort is quiet similar. Next, we insert the approximated quantities in (49) and taking the temporal evaluation

into account to get the fully discrete system given by

$$
\begin{aligned}
\delta\mathbf{V}_A \cdot M^{AB}\Big[(\boldsymbol{\varphi}_{Bn+1} - \boldsymbol{\varphi}_{Bn}) - \Delta t\, \mathbf{V}_{Bn+\frac{1}{2}}\Big] = 0 \\
\delta\boldsymbol{\varphi}_A \cdot \Big[\mathbf{M}_\rho^{AB}\, \frac{1}{\Delta t}(\mathbf{V}_{Bn+1} - \mathbf{V}_{Bn}) - \mathbf{F}_{\text{ext}}^A + \int_{\Omega_e} \mathbf{P}_{n+1}\, \nabla N^A \,\mathrm{d}V \\
+ \int_{\Omega_e} (\mathbf{P}_{n+1} - \mathbf{F}_{n+\frac{1}{2}}\, 2\, DW(\mathbf{C}_{n+\frac{1}{2}}))\, \frac{1}{j(\boldsymbol{\xi})} T(\boldsymbol{\mathcal{E}}(\boldsymbol{\xi}, \boldsymbol{\gamma}_{n+\frac{1}{2}}))^{\mathrm{T}}\, T^{\mathrm{T}}\, \nabla_0 N^A \,\mathrm{d}V \\
- \int_{\Omega_e} (\mathbf{P}_{n+1} - \mathbf{F}_{n+\frac{1}{2}}\, 2\, DW(\mathbf{C}_{n+\frac{1}{2}}))\, \frac{1}{j(\boldsymbol{\xi})} T(\boldsymbol{\mathcal{E}}_2(\boldsymbol{\xi}, \boldsymbol{\alpha}_{n+\frac{1}{2}}))^{\mathrm{T}}\, T^{\mathrm{T}}\, \nabla_0 N^A \,\mathrm{d}V \\
- \int_{\Omega_e} \mathbf{F}_{0\,n+\frac{1}{2}}^{-\mathrm{T}}\, T^{-\mathrm{T}}\, \boldsymbol{\mathcal{E}}(\boldsymbol{\xi}, \boldsymbol{\beta}_{n+1})\, T^{-1}\, (\widetilde{\mathbf{F}}_{n+\frac{1}{2}} - \mathbf{F}_{n+\frac{1}{2}})^{\mathrm{T}}\, \mathbf{F}_{0\,n+\frac{1}{2}}^{-\mathrm{T}}\, \nabla_0 N^A \,\mathrm{d}V\Big] = 0 \\
\delta\boldsymbol{\gamma}_0^v \cdot \Big[\int_{\Omega_e} \mathbf{P}_{n+1}^{\mathrm{v}} - \mathbf{F}_{n+\frac{1}{2}}^{\mathrm{v}}\, 2\, DW(\mathbf{C}_{n+\frac{1}{2}}^{\mathrm{v}})\,\mathrm{d}V\Big] = 0 \\
\delta\boldsymbol{\gamma} \cdot \Big[\int_{\Omega_e} \mathbf{B}_{\gamma_{n+\frac{1}{2}}} \Big(\mathbf{P}_{n+1}^{\mathrm{v}} - \mathbf{F}_{n+\frac{1}{2}}^{\mathrm{v}}\, 2\, DW(\mathbf{C}_{n+\frac{1}{2}}^{\mathrm{v}})\Big)\,\mathrm{d}V\Big] = 0 \\
\delta\boldsymbol{\alpha} \cdot \Big[\int_{\Omega_e} -\mathbf{B}_{\alpha_{n+\frac{1}{2}}} \Big(\mathbf{P}_{n+1}^{\mathrm{v}} - \mathbf{F}_{n+\frac{1}{2}}^{\mathrm{v}}\, 2\, DW(\mathbf{C}_{n+\frac{1}{2}}^{\mathrm{v}})\Big)\,\mathrm{d}V\Big] = 0 \\
\delta\boldsymbol{\beta}_0^v \cdot \Big[\int_{\Omega_e} \big(\widetilde{\mathbf{F}}_{n+1}^{\mathrm{v}} - \mathbf{F}_{n+1}^{\mathrm{v}}\big)\,\mathrm{d}V\Big] = 0 \\
\delta\boldsymbol{\beta} \cdot \Big[\int_{\Omega_e} \mathbf{B}_{\beta_{n+1}} \Big(\widetilde{\mathbf{F}}_{n+1}^{\mathrm{v}} - \mathbf{F}_{n+1}^{\mathrm{v}}\Big)\,\mathrm{d}V\Big] = 0
\end{aligned}
\tag{85}
$$

with

$$
M^{AB} = \int_{\Omega_e} N^A\, N^B \,\mathrm{d}V \tag{86}
$$

Due to the sophisticated element formulation, we have to go into detail with the temporal evaluation of the mixed quantities. As mentioned above, the mixed stress is assumed to be constant within a time-step. In the present formulation the mixed stress depends on the nodal quantities too, since we use the average deformation gradient. To avoid a violation of the angular momentum balance, we have to calculate the mixed stress by

$$
\mathbf{P}_{n+1} = \mathbf{P}(\boldsymbol{\varphi}_{n+\frac{1}{2}}, \boldsymbol{\beta}_{0n+1}, \boldsymbol{\beta}_{n+1}) \tag{87}
$$

The other quantities in (85) can be calculate as expected, such that

$$
\begin{aligned}
\mathbf{F}_{n+1} &= \mathbf{F}(\boldsymbol{\varphi}_{n+1}, \boldsymbol{\gamma}_{0n+1}, \boldsymbol{\gamma}_{n+1}, \boldsymbol{\alpha}_{n+1}) & \mathbf{F}_{0\,n+\frac{1}{2}} &= \mathbf{F}_0(\boldsymbol{\varphi}_{n+\frac{1}{2}}) \\
\mathbf{F}_{n+\frac{1}{2}} &= \mathbf{F}(\boldsymbol{\varphi}_{n+\frac{1}{2}}, \boldsymbol{\gamma}_{0n+\frac{1}{2}}, \boldsymbol{\gamma}_{n+\frac{1}{2}}, \boldsymbol{\alpha}_{n+\frac{1}{2}}) & \widetilde{\mathbf{F}}_{n+1} &= \widetilde{\mathbf{F}}(\boldsymbol{\varphi}_{n+1}) \\
& & \widetilde{\mathbf{F}}_{n+\frac{1}{2}} &= \widetilde{\mathbf{F}}(\boldsymbol{\varphi}_{n+\frac{1}{2}})
\end{aligned}
\tag{88}
$$

Note that the temporal evaluation of the mixed quantities formulated in tensor notation are similar to (87)-(88).

Subsequently, we linearize the non-linear system of equations (85) in a straightforward way. After a standard assembly operation, a static condensation process is possible. This reduces the computational effort drastically. Further details can be found in [26, 27].

Finally we point out that the conservation properties from the time discrete case are inherited by the present finite element method.

5 Numerical examples

In the following section we would like to point out the performance of the proposed mixed-enhanced finite element along with the newly developed EMC scheme.

5.1 Static investigation

The first numerical example deals with a static benchmark problem for nonlinear finite elements to demonstrate the performance in the nearly incompressible limit. We consider a 3d version of the so called Cook's membrane as depicted in Figure 1. The deformed configuration of the problem is shown in Figure 2. The tapered panel is clamped on the left and loaded by a shear load $\mathbf{p}$ on the right side, where

$$\mathbf{p} = \begin{bmatrix} 0 & 0 & 3 \end{bmatrix}^{\mathrm{T}} \tag{89}$$

A St. Venant-Kirchhoff material model with material parameters $E = 100$ and $\nu = 0.4999$ has been used. To demonstrate the superior performance we compare the Kasper & Taylor element (H1/ME9) with a standard displacement element (H1) and an enhanced element (H1/E9) by Simo & Armero [26]. As illustrated in Figure 3, the convergence with mesh refinement of the three elements under consideration is investigated. We consider the displacement of the top corner versus the number of elements per side. While the H1 elements locks drastically, the H1/E9 and H1/ME9 are in a good agreement. Thus we conclude, that the present formulation performs well, even in the incompressible limit and in bending dominated problems.

Further investigations about objectivity and plasticity and an Eigenvalue analysis can be found in [14, 15].

5.2 Dynamic investigation

The second example can be considered as a classical benchmark for the transient simulation of solids. According to Simo & Tarnow [28] we verify the algorithmic consistency of the developed EMC scheme along with its superior performance as shown in section 5.1.

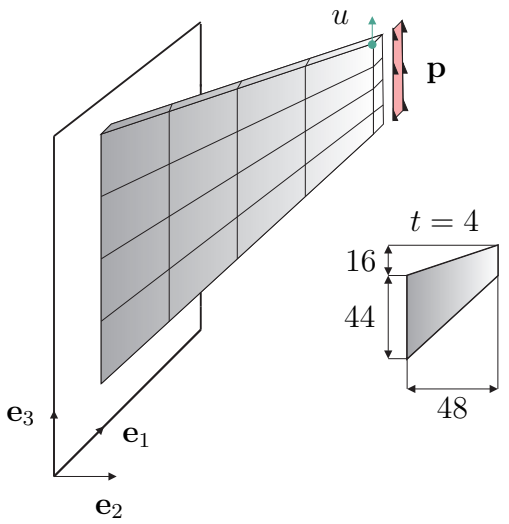

Figure 1: Cooks membrane problem. Geometry and boundary conditions

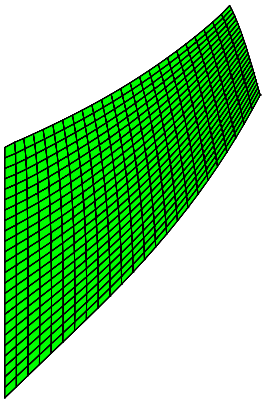

Figure 2: Cooks membrane problem. Deformed configuration

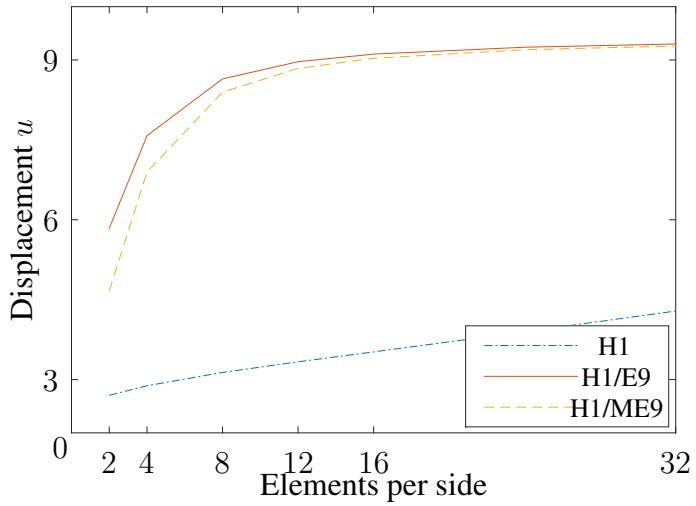

Figure 3: Study of convergence in static case. Quasi incompressible limit

Consider a flying L-shaped block with a constitutive behavior governed by a St. Venant-Kirchhoff material model. The material parameters are the Young Modulus $E = 2100$, the Poisson ratios $\nu = 0.4$ and the density $\rho_0 = 100$. Both, the initial geometry and the finite element mesh are illustrated in Figure 4. The L-shaped block has no Dirichlet boundary and pressure loads are acting on the block as shown in Figure 4. The time history of the external loads is illustrated in Figure 5. In this connection, the nodal

dead loads are given by

$$\begin{aligned} \mathbf{p}_1(t) &= f(t) \times \begin{bmatrix} -50 & -50 & -100 \end{bmatrix} \\ \mathbf{p}_2(t) &= f(t) \times \begin{bmatrix} 50 & 50 & 100 \end{bmatrix} \end{aligned} \tag{90}$$

The results of the EMC scheme are compared to those of the mid-point rule. All numerical simulation have been performed with a time-step size of $\Delta t = 0.25$. Note that after the loading phase the discrete system under consideration can be classified as autonomous Hamiltonian system with symmetry. Correspondingly, after $t \geq 1$, the total linear momentum, angular momentum and energy are conserved quantities. This is correctly reproduced by the EMC integrator (within the computational accuracy), whereas the mid-point rule exhibits numerical instabilities accompanied by an energy blow-up (see Figure 6). As depicted in Figure 7, the EMC scheme conserves the angular momentum exactly.

Eventually, the motion of the L-shape is illustrated in Figure 8 with a sequence of subsequent snapshots.

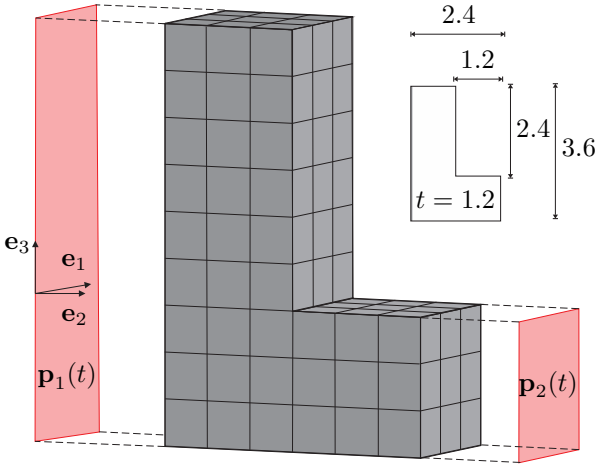

Figure 4: Flying L-Shape problem. Initial mesh configuration and dimensions

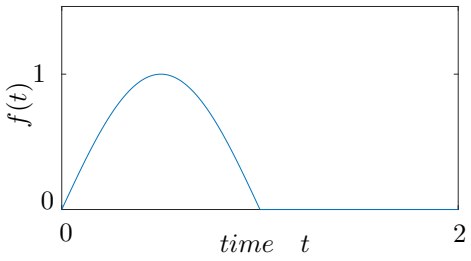

Figure 5: Time history of the external pressure

6 Conclusions

We developed a mixed variational formulation for nonlinear solid and structural dynamics which provides a natural framework for the EMC discretization in time. The underlying mixed variational equations were obtained as Euler-Lagrange equations of a mixed extension of Hamiltons principle. The Hu-Washizu type extension accommodates mixed finite elements based on independent interpolations of the displacements,

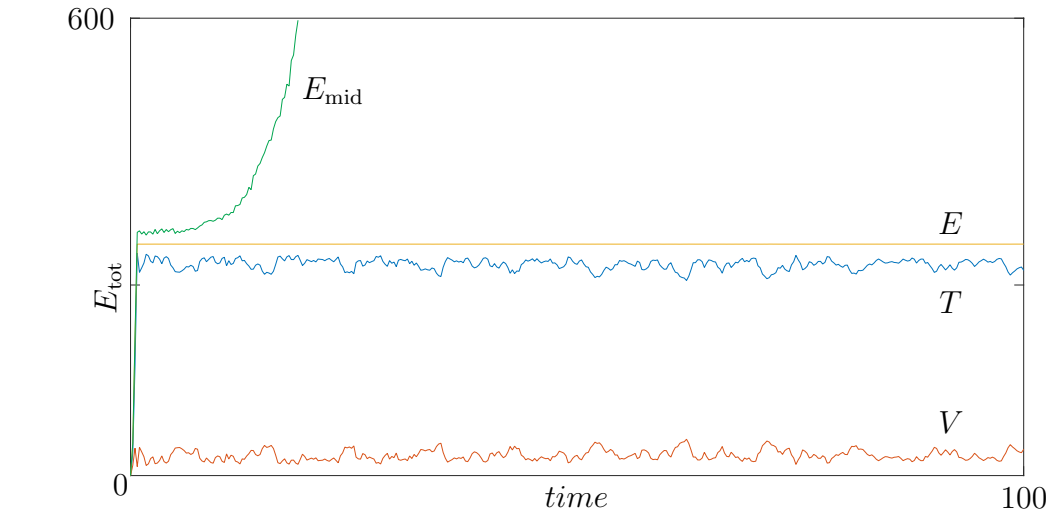

Figure 6: Time history of the total energy

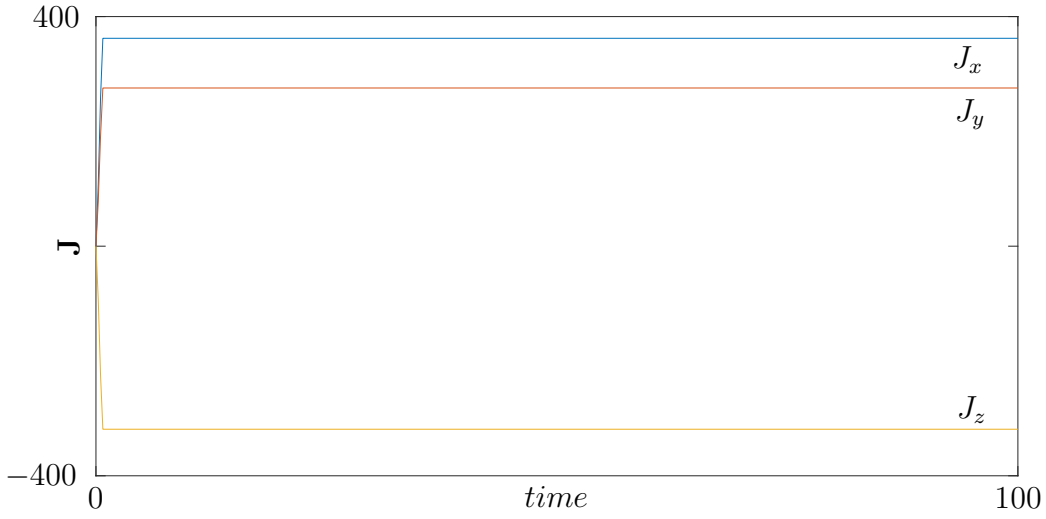

Figure 7: Time history of the angular momentum

the velocities, the deformation gradient, the right Cauchy-Green deformation tensor and both the first and the second Piola-Kirchhoff stresses.

We demonstrated, that the present framework is suitable even for more complicated formulations, like the mixed-enhanced element proposed by [15].

We show in Section 5.1, that the mixed-enhanced element performs well particularly

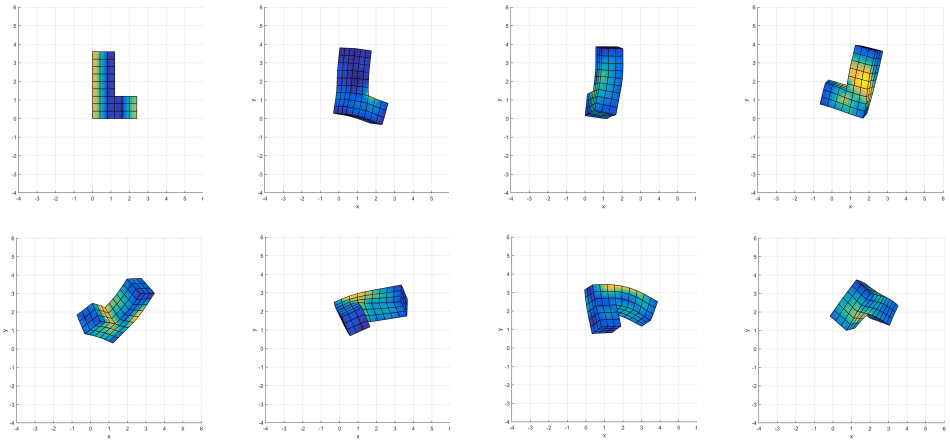

Figure 8: Snapshots of configurations at $t \in 0, 1, 2, 3, 4, 5, 6, 7, 8$

in the quasi-incompressible limit. The second numerical example, presented in section 5.2, shows that the EMC scheme leads to superior numerical stability properties compared to the common mid-point rule. While the conservation properties have been proven in the semi-discrete case and shown numerically, we still require a proof for the fully discrete system.

Accordingly, combining mixed finite element discretization in space with EMC discretization in time shows great promise for the design of numerical methods with superior coarse mesh accuracy in space and time. Thus, we obtain the possibility to use large time steps while still producing physically meaningful results, since the combination of EMC methods and mixed finite elements shows locking free response in non-linear dynamics.

Finally, we emphasize that many semidiscrete formulations of flexible bodies such as nonlinear continua, beams, and shells perfectly fit into the present framework, see [3]. Moreover, the present approach can be directly extended to flexible multibody dynamics as shown in [4].

Acknowledgement
Support for this research was provided by the Deutsche Forschungsgemeinschaft (DFG) under Grant BE 2285/9-1. This support is gratefully acknowledged.

A Appendix

A.1 Interpolation of mixed quantities

The maps for the three dimensional case are given by

$$\boldsymbol{\mathcal{E}}_1(\boldsymbol{\xi},\boldsymbol{\gamma}) = \begin{bmatrix} \xi_2\gamma_1 + \xi_3\gamma_2 + \xi_2\xi_3\gamma_3 & \xi_3\gamma_{10} & \xi_2\gamma_{14} \\ \xi_3\gamma_{11} & \xi_1\gamma_4 + \xi_3\gamma_5 + \xi_1\xi_3\gamma_6 & \xi_1\gamma_{12} \\ \xi_2\gamma_{15} & \xi_1\gamma_{13} & \xi_1\gamma_7 + \xi_2\gamma_8 + \xi_1\xi_2\gamma_9 \end{bmatrix}$$

$$\boldsymbol{\mathcal{E}}_2(\boldsymbol{\xi},\boldsymbol{\alpha}) = \begin{bmatrix} \xi_1\alpha_1 + \xi_1\xi_2\alpha_2 + \xi_1\xi_3\alpha_3 & 0 & 0 \\ 0 & \xi_2\alpha_4 + \xi_2\xi_3\alpha_5 + \xi_1\xi_2\alpha_6 & 0 \\ 0 & 0 & \xi_3\gamma_7 + \xi_2\xi_3\gamma_8 + \xi_1\xi_3\gamma_9 \end{bmatrix}$$

$$\boldsymbol{\mathcal{E}}_1(\boldsymbol{\xi},\boldsymbol{\beta}) = \begin{bmatrix} \xi_2\beta_1 + \xi_3\beta_2 + \xi_2\xi_3\beta_3 & \xi_3\beta_{10} & \xi_2\beta_{14} \\ \xi_3\beta_{11} & \xi_1\beta_4 + \xi_3\beta_5 + \xi_1\xi_3\beta_6 & \xi_1\beta_{12} \\ \xi_2\beta_{15} & \xi_1\beta_{13} & \xi_1\beta_7 + \xi_2\beta_8 + \xi_1\xi_2\beta_9 \end{bmatrix} \tag{91}$$

or equivalent, the interpolations in tensor form

$$\begin{aligned} \boldsymbol{\mathcal{E}}_1(\boldsymbol{\xi},\boldsymbol{\gamma}) &\xrightarrow{i,j\to i} \mathbf{E}_1(\boldsymbol{\xi})\,\boldsymbol{\gamma} \\ \boldsymbol{\mathcal{E}}_2(\boldsymbol{\xi},\boldsymbol{\alpha}) &\xrightarrow{i,j\to i} \mathbf{E}_1(\boldsymbol{\xi})\,\boldsymbol{\alpha} \\ \boldsymbol{\mathcal{E}}_1(\boldsymbol{\xi},\boldsymbol{\beta}) &\xrightarrow{i,j\to i} \mathbf{E}_1(\boldsymbol{\xi})\,\boldsymbol{\beta} \end{aligned} \tag{92}$$

$$\mathbf{E}_1(\boldsymbol{\xi}) = \begin{bmatrix} \eta & \zeta & \eta\zeta & 0 & 0 & 0 & 0 & 0 & 0 & 0 & 0 & 0 & 0 & 0 & 0 \\ 0 & 0 & 0 & \xi & \zeta & \xi\zeta & 0 & 0 & 0 & 0 & 0 & 0 & 0 & 0 & 0 \\ 0 & 0 & 0 & 0 & 0 & 0 & \xi & \eta & \xi\eta & 0 & 0 & 0 & 0 & 0 & 0 \\ 0 & 0 & 0 & 0 & 0 & 0 & 0 & 0 & 0 & \zeta & 0 & 0 & 0 & 0 & 0 \\ 0 & 0 & 0 & 0 & 0 & 0 & 0 & 0 & 0 & 0 & 0 & \xi & 0 & 0 & 0 \\ 0 & 0 & 0 & 0 & 0 & 0 & 0 & 0 & 0 & 0 & 0 & 0 & 0 & \eta & 0 \\ 0 & 0 & 0 & 0 & 0 & 0 & 0 & 0 & 0 & 0 & \zeta & 0 & 0 & 0 & 0 \\ 0 & 0 & 0 & 0 & 0 & 0 & 0 & 0 & 0 & 0 & 0 & 0 & \xi & 0 & 0 \\ 0 & 0 & 0 & 0 & 0 & 0 & 0 & 0 & 0 & 0 & 0 & 0 & 0 & 0 & \eta \end{bmatrix}$$

$$\mathbf{E}_2(\boldsymbol{\xi}) = \begin{bmatrix} \xi & \xi\eta & \xi\zeta & 0 & 0 & 0 & 0 & 0 & 0 \\ 0 & 0 & 0 & \eta & \eta\zeta & \xi\eta & 0 & 0 & 0 \\ 0 & 0 & 0 & 0 & 0 & 0 & \zeta & \eta\zeta & \xi\zeta \\ 0 & 0 & 0 & 0 & 0 & 0 & 0 & 0 & 0 \\ 0 & 0 & 0 & 0 & 0 & 0 & 0 & 0 & 0 \\ 0 & 0 & 0 & 0 & 0 & 0 & 0 & 0 & 0 \\ 0 & 0 & 0 & 0 & 0 & 0 & 0 & 0 & 0 \\ 0 & 0 & 0 & 0 & 0 & 0 & 0 & 0 & 0 \\ 0 & 0 & 0 & 0 & 0 & 0 & 0 & 0 & 0 \end{bmatrix} \tag{93}$$

REFERENCES

[1] F. Armero. Assumed strain finite element methods for conserving temporal integrations in non-linear solid dynamics. *Int. J. Numer. Meth. Engng*, 74(12):1795–1847, 2008.

[2] F. Armero and I. Romero. Energy-dissipative momentum-conserving time-stepping algorithms for the dynamics of nonlinear Cosserat rods. *Computational Mechanics*, 31:3–26, 2003.

[3] P. Betsch and A. Janz. An energy-momentum consistent method for transient simulations with mixed finite elements developed in the framework of geometrically exact shells. Accepted for publication in Int. J. Numer. Meth. Engng.

[4] P. Betsch and N. Sänger. On the use of geometrically exact shells in a conserving framework for flexible multibody dynamics. *Comput. Methods Appl. Mech. Engrg.*, 198:1609–1630, 2009.

[5] P. Betsch and P. Steinmann. A DAE approach to flexible multibody dynamics. *Multibody System Dynamics*, 8:367–391, 2002.

[6] P. Betsch and P. Steinmann. Constrained dynamics of geometrically exact beams. *Computational Mechanics*, 31:49–59, 2003.

[7] C.L. Bottasso, O.A. Bauchau, and J.-Y. Choi. An energy decaying scheme for nonlinear dynamics of shells. *Comput. Methods Appl. Mech. Engrg.*, 191(27-28):3099–3121, 2002.

[8] B. Brank, J. Korelc, and A. Ibrahimbegović. Dynamics and time-stepping schemes for elastic shells undergoing finite rotations. *Computers and Structures*, 81(12):1193–1210, 2003.

[9] U. Galvanetto and M.A. Crisfield. An energy-conserving co-rotational procedure for the dynamics of planar beam structures. *Int. J. Numer. Meth. Engng*, 39:2265–2282, 1996.

[10] O. Gonzalez. Time integration and discrete Hamiltonian systems. *J. Nonlinear Sci.*, 6:449–467, 1996.

[11] O. Gonzalez. Exact energy and momentum conserving algorithms for general models in nonlinear elasticity. *Comput. Methods Appl. Mech. Engrg.*, 190(13-14):1763–1783, 2000.

[12] O. Gonzalez and J.C. Simo. On the stability of symplectic and energy-momentum algorithms for non-linear Hamiltonian systems with symmetry. *Comput. Methods Appl. Mech. Engrg.*, 134:197–222, 1996.

[13] C. Hesch and P. Betsch. Energy-momentum consistent algorithms for dynamic thermomechanical problems – application to mortar domain decomposition problems. *Int. J. Numer. Meth. Engng*, 86(11):1277–1302, 2011.

[14] E.P. Kasper and R.L. Taylor. A mixed-enhanced strain method. Part I: Geometrically linear problems. *Computers and Structures*, 75(3):237–250, 2000.

[15] E.P. Kasper and R.L. Taylor. A mixed-enhanced strain method. Part II: Geometrically nonlinear problems. *Computers and Structures*, 75(3):251–260, 2000.

[16] D. Kuhl and E. Ramm. Time integration in the context of energy control and locking free finite elements. *Archives of Computational Methods in Engineering. State of the Art Reviews*, 7(3):299–332, 2000.

[17] T.A. Laursen and X.N. Meng. A new solution procedure for application of energy-conserving algorithms to general constitutive models in nonlinear elastodynamics. *Comput. Methods Appl. Mech. Engrg.*, 190:6309–6322, 2001.

[18] E.V. Lens and A. Cardona. A nonlinear beam element formulation in the framework of an energy preserving time integration scheme for constrained multibody systems dynamics. *Computers and Structures*, 86(1-2):47–63, 2008.

[19] S. Leyendecker, P. Betsch, and P. Steinmann. Objective energy-momentum conserving integration for the constrained dynamics of geometrically exact beams. *Comput. Methods Appl. Mech. Engrg.*, 195:2313–2333, 2006.

[20] C. Miehe and J. Schröder. Energy and momentum conserving elastodynamics of a non-linear brick-type mixed finite shell element. *Int. J. Numer. Meth. Engng*, 50:1801–1823, 2001.

[21] L.A. Pars. *A treatise on analytical dynamics*. Heinemann, 1965.

[22] I. Romero. An analysis of the stress formula for energy-momentum methods in nonlinear elastodynamics. *Computational Mechanics*, 50:603–610, 2012.

[23] I. Romero and F. Armero. Numerical integration of the stiff dynamics of geometrically exact shells: an energy-dissipative momentum-conserving scheme. *Int. J. Numer. Meth. Engng*, 54:1043–1086, 2002.

[24] I. Romero and F. Armero. An objective finite element approximation of the kinematics of geometrically exact rods and its use in the formulation of an energy-momentum conserving scheme in dynamics. *Int. J. Numer. Meth. Engng*, 54:1683–1716, 2002.

[25] C. Sansour, T.L. Nguyen, and M. Hjiaj. An energy-momentum method for in-plane geometrically exact Euler-Bernoulli beam dynamics. *Int. J. Numer. Meth. Engng*, 102:99–134, 2015.

[26] J.C. Simo and F. Armero. Geometrically nonlinear enhanced strain mixed methods and the method of incompatible modes. *Int. J. Numer. Meth. Engng*, 33:1413–1449, 1992.

[27] J.C. Simo, F. Armero, and R.L. Taylor. Improved versions of assumed enhanced strain tri-linear elements for 3d finite deformation problems. *Comput. Methods Appl. Mech. Engrg.*, 110:359–386, 1993.

[28] J.C. Simo and N. Tarnow. The discrete energy-momentum method. Conserving algorithms for nonlinear elastodynamics. *Z. angew. Math. Phys. (ZAMP)*, 43:757–792, 1992.

[29] J.C. Simo and N. Tarnow. A new energy and momentum conserving algorithm for the nonlinear dynamics of shells. *Int. J. Num. Meth. Engng*, 37:2527–2549, 1994.

[30] J.C. Simo, N. Tarnow, and M. Doblare. Non-linear dynamics of three-dimensional rods: Exact energy and momentum conserving algorithms. *Int. J. Numer. Meth. Engng*, 38:1431–1473, 1995.

[31] K. Washizu. *Variational Methods in Elasticity & Plasticity*. Pergamon Press, 3rd edition, 1982.

[32] H.G. Zhong and M.A. Crisfield. An energy-conserving co-rotational procedure for the dynamics of shell structures. *Eng. Comp.*, 15:552–576, 1998.